

1 ***Neural correlates and determinants of approach-avoidance conflict in***
2 ***the prelimbic prefrontal cortex***

3
4 Fernandez-Leon, J.A.^{#1,2}; Engelke, D.S.^{#1}; Aquino-Miranda, G.^{#1}; Goodson, A.^{1,3};
5 Rasheed, M.N.¹; Do-Monte, F.H.^{1,3*}.

6
7
8
9
10 ¹ Dept. of Neurobiology & Anatomy, The University of Texas Health Science Center,
11 Houston, TX77030, USA;

12
13 ² Current Affiliation: Exact Sciences Faculty, CIFICEN (UNCPBA-CONICET-CICPBA) &
14 INTIA (UNCPBA-CICPBA), Tandil 7000, Buenos Aires, Argentina;

15
16 ³ Rice University, Houston, TX77030, USA

17
18 # These authors contributed equally to this work

19
20 *Corresponding author:

21 Fabricio H. Do Monte, DVM, PhD.
22 Department of Neurobiology and Anatomy, McGovern Medical School,
23 The University of Texas Health Science Center at Houston
24 6431 Fannin Street, Room 7.166, Houston, Texas 77030
25 Phone: 713-500-5613
26 Email: fabricio.h.domonte@uth.tmc.edu

27
28
29
30
31
32
33
34
35
36
37
38
39
40
41
42
43
44

Keywords: Prelimbic prefrontal cortex, electrophysiology, optogenetics, fear, reward, decision-making.

45 **ABSTRACT**

46

47

48 The recollection of environmental cues associated with threat or reward allows animals
49 to select the most appropriate behavioral responses. Neurons in the prelimbic cortex
50 (PL) respond to both threat- and reward-associated cues. However, it remains unknown
51 whether PL regulates threat-avoidance vs. reward-approaching responses when an
52 animals' decision depends on previously associated memories. Using a conflict model
53 in which male Long-Evans rats retrieve memories of shock- and food-paired cues, we
54 observed two distinct phenotypes during conflict: i) rats that continued to press a lever
55 for food (*Pressers*); and ii) rats that exhibited a complete suppression in food seeking
56 (*Non-Pressers*). Single-unit recordings revealed that increased risk-taking behavior in
57 *Pressers* is associated with persistent food-cue responses in PL, and reduced
58 spontaneous activity in PL glutamatergic (PL^{GLUT}) neurons during conflict. Activating
59 PL^{GLUT} neurons in *Pressers* attenuated food-seeking responses in a neutral context,
60 whereas inhibiting PL^{GLUT} neurons in *Non-Pressers* reduced defensive responses and
61 increased food approaching during conflict. Our results establish a causal role for
62 PL^{GLUT} neurons in mediating individual variability in memory-based risky decision
63 making by regulating threat-avoidance vs. reward-approach behaviors.

64

65

66

67

68

69 INTRODUCTION

70 The brain's ability to identify and discriminate cues associated with threat or reward
71 allows organisms to respond appropriately to changes in the environment (Schultz,
72 2015; Hu, 2016). Animals respond to threatening cues with a series of defensive
73 behaviors including avoidance responses that decrease their chances of being exposed
74 to aversive outcomes (McNaughton and Corr, 2014; Krypotos et al., 2015; Cain, 2019).
75 In contrast, reward cues have attractive and motivational properties that elicit approach
76 behavior (Robinson and Flagel, 2009; Morales and Berridge, 2020). When animals are
77 exposed to threat and reward cues simultaneously, an approach-avoidance conflict
78 emerges, and decision-making processes are recruited to resolve the situation (Kirlic et
79 al., 2017; Barker et al., 2019). While many studies have investigated the neural
80 mechanisms that control threat-avoidance and reward-approach independently of each
81 other, it is unclear how the brain uses previously learned information to regulate the
82 opposing behavioral drives of avoiding threats and seeking rewards during a conflict
83 situation.

84 Neurons in the prelimbic (PL) subregion of the medial prefrontal cortex (mPFC)
85 change their firing rates in response to cues that predict either threat or reward (Baeg et
86 al., 2001; Burgos-Robles et al., 2009; Burgos-Robles et al., 2013; Moorman and Aston-
87 Jones, 2015; Dejean et al., 2016; Otis et al., 2017). Accordingly, activity in PL neurons
88 is necessary for the retrieval of both food- and threat-associated memories (Sierra-
89 Mercado et al., 2011; Courtin et al., 2014; Sangha et al., 2014; Do-Monte et al., 2015;
90 Otis et al., 2017). PL neurons are reciprocally connected with the basolateral nucleus of
91 the amygdala (BLA) (McDonald, 1991; Vertes, 2004), a region implicated in the

92 detection of threats or rewards (Amir et al., 2015; Namburi et al., 2015; Beyeler et al.,
93 2016; Zhang et al., 2020). During a risky foraging task in rats, dynamic modifications in
94 the activity of PL and BLA neurons correlate with the detection of imminent threats and
95 the defensive readiness for action (Kim et al., 2018; Kyriazi et al., 2020). In addition,
96 during a modified Pavlovian cue discrimination task involving footshocks as punishment,
97 increased activity in the BLA-PL pathway is sufficient and necessary for the expression
98 of freezing responses (Burgos-Robles et al., 2017), a passive form of defensive
99 behavior. Conversely, inhibitory signaling in PL neurons correlates with threat
100 avoidance (Diehl et al., 2018), an active form of defensive behavior. While these studies
101 suggest a potential role of PL during motivational conflict involving states of certainty
102 (i.e., imminent threats), it is unknown whether changes in PL activity underlie the
103 behavioral variability in approach-avoidance responses under states of uncertainty,
104 when animal's decision depends entirely on the retrieval of previously associated
105 memories. It is also unclear whether PL activity is necessary to coordinate appropriate
106 behavioral responses during conflict, and if so, which sub-types of PL neurons govern
107 the competing demands of approaching rewards vs. avoiding potential threats.

108 To address these questions, we designed an approach-avoidance conflict test
109 that assesses the ability of rats to remember cues previously associated with either food
110 or footshocks to make a behavioral decision. Using a combination of optogenetics and
111 single-unit recordings, we investigated rats' individual variability in reward seeking and
112 defensive responses during the conflict test and correlated their behaviors (e.g.
113 freezing, avoidance, risk-assessment) with the firing rate of photoidentified
114 glutamatergic and GABAergic neurons in PL. We then examined the role of PL neurons

115 in risky decision-making by optogenetically manipulating PL activity with high temporal
116 resolution and cell-type specificity during the conflict test.

117

118 **RESULTS**

119 **Rats show individual variability in reward-seeking and defensive responses** 120 **during the approach-avoidance conflict test.**

121 To investigate the motivational conflict between approaching rewards and avoiding
122 potential threats, we established a behavioral model in which rats need to balance food
123 seeking with conditioned defensive responses based on their memories of previously
124 acquired cues. Food-restricted rats (18 g of chow per day) were initially placed in an
125 operant box and trained to press a lever for sucrose in the presence of audiovisual cues
126 that signaled the availability of food. Each lever press during the audiovisual cue
127 presentation resulted in the delivery of a sucrose pellet into a nearby dish (see Methods
128 for details). When rats reached 50% of discrimination during cued food-seeking, they
129 began lever-pressing for sucrose preferentially during the audiovisual cues
130 (**Supplementary Fig. 1A-B**). During the habituation day, rats were placed in an odor
131 arena and familiarized with the food cues and the neutral odor amyl acetate (see
132 Methods for details). Next, to pair the odor cue with an aversive stimulus, rats were
133 exposed to an olfactory threat conditioning training (Day 1). Animals were placed in an
134 operant box (conditioning box; **Fig. 1A left**) previously connected to an olfactometer
135 and habituated to one odor presentation (amyl acetate, 30 s) without footshock,
136 followed by five odor presentations of the same odor that co-terminated with an

137 electrical footshock (0.7 mA, 1 s duration, 270-390 s inter-trial intervals, **Fig. 1A far-**
138 **left**). Food cues (30 s duration) were presented during the odor intervals to assess how
139 threat conditioning alters lever press responses. Rats showed robust defensive
140 responses during the threat conditioning training, as evidenced by an increase in
141 freezing (Shapiro Wilk normality test, $p < 0.001$, Friedman Test, Friedman statistic =
142 84.08, $p < 0.001$; Dunn's *post-hoc*, $p < 0.001$) during the conditioned odor presentation
143 (**Fig. 1B**), and a decrease in lever presses (**Fig. 1C**, Shapiro Wilk normality test, $p <$
144 0.001 , Friedman Test, Friedman statistic = 35.11, $p < 0.001$; Dunn's *post-hoc*, $p <$
145 0.001) and an increase in the latency to press the lever (**Fig. 1D**, Shapiro Wilk normality
146 test, $p < 0.001$, Friedman Test, Friedman statistic = 29.45, $p < 0.001$; Dunn's *post-hoc*,
147 $p < 0.001$) during the presentation of the food cues across trials. After rats have
148 acquired the reward and threat associations, they were returned to the same odor arena
149 in which they were previously habituated and exposed to a test session (Day 2) (**Fig 1A,**
150 **right**). The test session consisted of three different phases: (i) a *Reward Phase*, in
151 which only the audiovisual cues signaling the availability of food were presented; (ii) an
152 *Odor Phase*, in which only the conditioned odor was presented, and a (iii) *Conflict*
153 *phase*, in which both the food cues and the conditioned odor were presented
154 simultaneously (**Fig 1A, far-right**).

155 During the reward phase, rats spent ~40% of the time in the food area and
156 pressed the lever for food in ~95% of the food cue trials, without exhibiting significant
157 defensive behaviors (**Fig. 1E-J**). Introduction of the shock-paired odor during the odor
158 phase reduced the percentage of time rats spent in the food area to ~15% (Shapiro Wilk
159 normality test, $p < 0.05$, Friedman Test, Friedman statistic = 32.19, $p < 0.001$, Dunn's

160 *post-hoc*, $p < 0.001$) and increased defensive behaviors characterized by freezing
161 (Shapiro Wilk normality test, $p < 0.05$, Friedman Test, Friedman statistic = 40.46, $p <$
162 0.001, Dunn's *post-hoc*, $p < 0.001$), avoidance (Shapiro Wilk normality test, $p < 0.05$,
163 Friedman Test, Friedman statistic = 31.67, $p < 0.001$, Dunn's *post-hoc*, $p < 0.001$), and
164 risk-assessment responses (Shapiro Wilk normality test, $p < 0.05$, Friedman Test,
165 Friedman statistic = 29.86, $p < 0.001$, Dunn's *post-hoc*, $p < 0.001$; **Fig. 1E-H**). These
166 defensive behaviors were attenuated by the introduction of food cues during the conflict
167 phase, as evidenced by a reduction in the percentage of time avoiding the conditioned
168 odor (**Fig. 1F**, Dunn's *post-hoc*, $p = 0.0031$) and an increase in the percentage of time
169 approaching the food area (**Fig. 1H**, Dunn's *post-hoc*, $p < 0.001$). This indicates that the
170 concomitant presentation of food cues and shock-paired odor induced a behavioral
171 conflict in the animals. Interestingly, when we analyzed the percentage of rewarded
172 presses during the conflict phase (**Fig. 1J**), two behavioral phenotypes emerged: *i*) rats
173 that continued to press the lever for food in the presence of the threatening odor
174 (*Pressers*, **Fig. 1K**); and *ii*) rats that showed a complete suppression in lever presses in
175 the presence of the threatening odor (*Non-Pressers*, **Fig. 1L**). We then separated the
176 animals into two different groups based on whether the animals pressed the lever or not
177 during the conflict phase and compared their behaviors during the entire test session
178 (**Fig. 1K-R, Supplementary Movie 1**). *Pressers* and *Non-Pressers* exhibited similar
179 behavioral responses during the reward phase (all p 's > 0.05). However, during the odor
180 and the conflict phases, *Pressers* showed a lower percentage of time exhibiting freezing
181 (**Fig. 1M**, two-way repeated measures ANOVA, interaction - $F_{(2, 60)} = 29.54$ $p < 0.001$,
182 Bonferroni *post-hoc* test - odor phase, $p < 0.001$; conflict phase, $p < 0.001$) and

183 avoidance responses (**Fig. 1N**, Two-way repeated measures ANOVA, interaction- $F_{(2, 60)}$)
184 = 23.27, $p < 0.001$, Bonferroni *post-hoc* test - odor phase, $p < 0.001$; conflict phase, $p <$
185 0.001), and a greater percentage of time approaching the food area (**Fig. 1P**, two-way
186 repeated measures ANOVA, interaction- $F_{(2, 60)} = 22.49$, $p < 0.001$, Bonferroni *post-hoc*
187 test - odor phase, $p = 0.0453$; conflict phase, $p < 0.001$) when compared to *Non-*
188 *Pressers* during both the odor and the conflict phases. A principal component analysis
189 (PCA) showed that PC1 explained most of the variance of the data ($> 60\%$), with
190 latency to press the lever and percentage of time in the food area being the two
191 variables that most contributed to PC1 (0.54 and 0.52, respectively). Because these two
192 variables are directly associated with lever presses, the PCA results support our binary
193 classification of rats into *Pressers* and *Non-Pressers* based on whether they pressed
194 the lever or not during the conflict phase.

195 Subsequent behavioral analyses demonstrated that these two individual
196 phenotypes were not due to prior differences in reward-seeking motivation or odor-
197 shock association because *Pressers* and *Non-Pressers* showed similar lever pressing
198 rates during the cued food-seeking training (**Supplementary Fig. 1A-B**; Two-way
199 repeated measures ANOVA, interaction- $F_{(1, 55)} = 0.1065$, $p = 0.7454$) and threat
200 conditioning phase (**Supplementary Fig. 1C**; Two-way repeated measures ANOVA,
201 $F_{(1,51)} = 0.265$, $p = 0.608$), as well as the same freezing levels (Two-way repeated
202 measures ANOVA, $F_{(1,51)} = 3.737$, $p = 0.058$) and maximum speed (Two-way repeated
203 measures ANOVA, $F_{(1,51)} = 6.538e007$, $p = 0.999$) in response to the shock-paired odor
204 during the threat conditioning phase (**Supplementary Fig. 1D-E**). The two phenotypes
205 might not be attributed to prior differences in the relative salience of the odor and the

206 audiovisual cues because *Pressers* and *Non-Pressers* spent the same time
207 investigating the odor and exhibited the same response latency to the audiovisual cues
208 during the pre-conditioning period (**Supplementary Fig. 1F-G**; Unpaired student's t-
209 test, $t = 0.43$, $p = 0.665$ and Unpaired Student's t-test, $t = 0.55$, $p = 0.578$, respectively).
210 Although *Non-Pressers* exhibited higher freezing levels during pre-odor trials 3 and 4 of
211 the threat conditioning phase (**Supplementary Fig. 1H**, $F_{(5, 250)} = 3.038$, $p = 0.011$,
212 Bonferroni's post-hoc $p < 0.05$), freezing responses before the first food cue and odor
213 presentation were the same during the test day, indicating similar contextual
214 discrimination between the two groups (**Supplementary Fig. 1I**, Shapiro Wilk normality
215 test, $p < 0.05$, Mann-Whitney test, $U = 248$, $p = 0.113$). A minute-by-minute analysis
216 during the odor phase demonstrated that behavioral differences in freezing (Two-way
217 repeated measures ANOVA, Group $F_{(1,50)} = 13.07$, $p < 0.001$; Interaction, $F_{(9,450)} =$
218 1.327 , $p = 0.220$), avoidance (Group $F_{(1,50)} = 20.31$, $p < 0.001$; Interaction, $F_{(9,450)} =$
219 2.109 , $p = 0.027$, Bonferroni post-hoc min 1 vs. min 10 $p > 0.999$), and time spent in the
220 food area (Group $F_{(1, 50)} = 117.5$, $p = 0.001$; Interaction, $F_{(9, 450)} = 0.573$, $p = 0.819$)
221 between *Pressers* and *Non-Pressers* were already observed in the beginning of the
222 odor phase, and these behaviors remained constant in both groups across the entire
223 duration of the session (**Supplementary Figure 1J-L**), ruling out the possibility that the
224 group differences were caused by extinction of the odor-shock association in *Pressers*.

225 Together, our results demonstrate that our conflict model is a suitable paradigm
226 to investigate the interactions between reward- and threat-associated memories. Given
227 that rats exhibit individual differences in food seeking and defensive responses during
228 the test session, we next took advantage of the two observed phenotypes to examine

229 the neuronal correlates of risk-taking (*Pressers*) and risk-avoiding (*Non-Pressers*)
230 behaviors in PL neurons.

231

232 **PL neurons respond differently to reward cues in *Pressers* vs. *Non-Pressers***
233 **during the conflict test.**

234 To investigate the role of PL neurons in regulating food-approach and threat-avoidance
235 responses, we performed single-unit recordings across the different phases of the
236 conflict test (**Fig. 2A**). We aligned the activity of PL neurons to the onset of the food
237 cues during the reward phase and tracked the firing rates of the same cells during the
238 conflict phase. Using the behavioral classification shown in **Fig. 1J**, we separated the
239 animals into *Pressers* or *Non-pressers* and compared changes in PL activity in
240 response to food cues during the reward and conflict phases (**Fig. 2B-V**). When PL
241 activity was time-locked to the onset of the food cues during the reward phase, *Pressers*
242 showed a higher number of food-cue responsive neurons than *Non-Pressers* (**Fig. 2C-D**
243 **vs. Fig. 2M-N**; Fisher Exact Test, 33% in *Pressers* vs. 21% in *Non-Pressers*, $p =$
244 0.0418), with a similar proportion of excitatory and inhibitory responses between the two
245 groups (Fisher Exact Test, $p = 0.073$ for excitatory, $p = 0.571$ for inhibitory). During the
246 conflict phase, both *Pressers* and *Non-Pressers* showed a significant reduction in the
247 number of food-cue responsive neurons (**Fig. 2C-D vs. 2M-N**; Fisher Exact Test, from
248 33% to 14% in *Pressers*, $p < 0.001$; from 21% to 6% in *Non-Pressers*, $p = 0.0086$), as
249 well as in the magnitude of excitatory food-cue responses compared to the reward
250 phase (**Fig. 2E inset and Fig. 2O inset**, Shapiro-Wilk normality test, $p < 0.001$,
251 Wilcoxon test, *Pressers* – $W = -824$, $p < 0.001$; *Non-Pressers* – $W = -37$, $p = 0.032$),

252 suggesting that PL neurons can distinguish between reward and conflict situations (**Fig.**
253 **2G vs. 2H and 2R vs. 2S**).

254 Using a temporal frequency separation of the food cue responses into transient
255 (< 600 ms duration) and sustained (\geq 900 ms duration) activity (Bezdudnaya et al.,
256 2006), we revealed that *Pressers* display a higher proportion of sustained excitatory
257 responses during the reward phase, when compared to *Non-Pressers* (**Fig. 2F vs. 2P**,
258 50 % in *Pressers* vs. 10% in *Non-Pressers*, Fisher Exact Test, $p = 0.032$). In addition,
259 *Pressers* showed a higher magnitude of inhibitory food-cue responses during the
260 reward phase (**Fig. 2I** blue bar inset vs. **2S** blue bar inset, Shapiro-Wilk normality test, p
261 < 0.001 , Mann-Whitney test, $U = 50$, $p = 0.0045$) and, in contrast to *Non-Pressers*, such
262 responses were attenuated during the conflict phase (**Fig. 2I inset vs. Fig. 2S inset**,
263 *Pressers*, Shapiro-Wilk normality test, $p < 0.001$, Wilcoxon test – $W = 367$, $p < 0.001$;
264 *Non-Pressers*, Paired Student's t-test, $t = 0.59$, $p = 0.569$). A correlation analysis during
265 the conflict phase revealed that food cue-evoked excitatory PL activity in *Pressers* was
266 inversely correlated with lever press latency, indicating that the higher the firing rate of
267 food-cue responsive cells after the onset of the audiovisual cues, the quicker the
268 animals searched for rewards (**Supplementary Fig. 2A-B**).

269 Next, we time-locked the activity of PL neurons to the onset of the food cues
270 during the conflict phase. Both *Pressers* and *Non-Pressers* show the same number of
271 food-cue responsive neurons (**Supplementary Fig. 3A-B vs. Supplementary Fig. 3K-**
272 **L**, 28% in *Pressers* vs. 20% in *Non-Pressers*, Fisher Exact Test, $p = 0.391$) and the
273 same magnitude of excitatory food-cue responses during the conflict phase
274 (**Supplementary Fig. 3C, E, F vs. Supplementary Fig. 3M, O, P**; area under the

275 curve, *Pressers* vs. *Non-Pressers*, Shapiro-Wilk normality test, $p < 0.001$, Mann-
276 Whitney, $U = 107$, $p = 0.123$). However, in *Pressers*, 42% of excitatory food-cue
277 responses showed sustained activity during the conflict phase whereas such responses
278 were completely absent in *Non-Pressers* (**Supplementary Fig. 3D vs. Supplementary**
279 **Fig. 3N**, Fisher Exact Test, $p = 0.018$).

280 In addition to food cue responses, we observed a significant proportion of PL
281 neurons that changed their firing rates in response to lever presses (23%) or rewarded
282 food dish entries (16%, **Supplementary Fig. 4A-N**). A longitudinal tracking of PL
283 activity throughout the reward phase demonstrated that most PL responsive neurons
284 changed their activities selectively to food cues, lever presses, or food dish entries, with
285 a smaller number of cells responding during two or more of these events
286 (**Supplementary Fig. 4O**). This observation suggests that PL neurons exhibit a
287 heterogeneous pattern of activity during reward-seeking behavior, consistent with a
288 recent study using calcium imaging recordings from PL neurons in head-fixed mice
289 ([Grant et al., 2021](#)).

290 To further explore whether changes in activity dynamics of PL neurons differ
291 between *Pressers* and *Non-Pressers*, we compared the spontaneous firing rate of the
292 neurons before vs. after each phase of the test session (**Supplementary Fig. 5A**).
293 While *Pressers* showed the same proportion of neurons excited and inhibited across the
294 different phases (Fisher Exact Test, all p 's > 0.05), *Non-Pressers* exhibited a significant
295 increase in the proportion of neurons excited during the conflict phase (**Supplementary**
296 **Fig. 5C**, Fisher Exact Test, $p = 0.015$). This suggests that increased spontaneous
297 activity in PL neurons during the conflict phase may be associated with the complete

298 suppression in lever presses observed in *Non-Pressers* (**Fig. 1J**). Collectively, these
299 results suggest that differences in the number and magnitude of excitatory food cue
300 responses, as well as in the spontaneous activity of PL neurons during the conflict test,
301 may contribute to the individual differences in risky decision making observed between
302 the two behavioral phenotypes.

303

304 **Different subsets of PL neurons signal freezing, avoidance, and risk-assessment**
305 **behaviors in both *Pressers* and *Non-pressers*.**

306 To investigate whether PL activity correlates with the expression of distinct defensive
307 behaviors during the test session, we used a pose estimation algorithm (DeepLabCut,
308 see Methods for details) to identify the onset of freezing, avoidance or risk-assessment
309 responses and align these time points with the activity of PL neurons. We found that a
310 small percentage of PL neurons changed their firing rates during the onset of freezing
311 (**Fig. 3A**), avoidance (**Fig. 3B**), or risk-assessment (**Fig. 3C**) behaviors in both *Pressers*
312 and *Non-Pressers*, with a similar proportion of excitatory and inhibitory responses being
313 observed in the two groups (**Fig. 3A-I**). Interestingly, most PL responsive neurons
314 (80%) changed their activities exclusively during the onset of one of these three
315 behaviors, with a reduced number of avoidance-responsive cells also responding during
316 the onset of risk-assessment behavior (**Fig. 3J-M**). Moreover, a smaller fraction of PL
317 neurons changed their firing rates 600 ms before the onset of either freezing, avoidance
318 or risk-assessment responses in both *Pressers* and *Non-Pressers* (**Supplementary**
319 **Fig. 6A-M**), indicating that some PL neurons can anticipate an animal's defensive
320 behavior during the test. Overall, these results suggest that different subsets of PL

321 neurons signal distinct behavioral outcomes during a conflict situation, with only a
322 reduced number of PL neurons encoding the aversive salience of environmental cues
323 independently of the defensive response expressed by the animal.

324

325 ***Pressers* and *Non-Pressers* show significant differences in delta and theta**
326 **oscillations in PL**

327 Previous studies have shown that oscillations in mPFC neuronal activity at
328 different frequency bands correlate with distinct behavioral states in both rodents and
329 humans ([Narayanan et al., 2013](#); [Harris and Gordon, 2015](#)). Neural oscillations in the
330 mPFC emerge from the network of excitatory and inhibitory synaptic connections and
331 are thought to contribute to neural communication when subjects engage in reward and
332 threat memory tasks ([Hyman et al., 2011](#); [Likhtik and Paz, 2015](#); [Park and Moghaddam,](#)
333 [2017](#); [Widge et al., 2019](#)). To investigate whether *Pressers* and *Non-Pressers* show
334 significant differences in PL oscillations during conflict, we recorded local field potentials
335 (LFPs) from PL neurons and calculated the average of power spectral density (PSD) at
336 different frequencies across the test session. After comparing the PSD contribution for
337 each frequency range in *Pressers* and *Non-Pressers*, we observed that most of the
338 signal originated from the delta (0-4 Hz) and theta (4-10 Hz) bands, with a much smaller
339 contribution coming from the alpha (10-14 Hz), beta (14-35 Hz), and gamma (>35 Hz)
340 frequencies (**Fig. 4A**). We therefore focused our analyses on these two bands and
341 found that *Pressers* displayed increased power in the delta band, whereas *Non-*
342 *Pressers* exhibited increased power in the theta band during the three phases of the
343 test session (**Fig. 4B-C**, Paired Student's t-test of Area Under the Curve, all p's <

344 0.001). Differences between *Pressers* and *Non-Pressers* were also observed in the
345 time-frequency domain through changes in the log of PSD for delta and theta bands
346 across the different phases (**Fig. 4D-E**, Paired Student's t-test of Area Under the Curve,
347 all p's < 0.001). These results indicate that phenotypic differences in approach-
348 avoidance conflict are associated with distinct oscillatory frequencies in PL.

349

350 **In pressers, PL^{GLUT} neurons show reduced spontaneous activity during the**
351 **conflict phase.**

352 The rodent mPFC, including PL, is primarily composed of excitatory
353 glutamatergic cells that correspond to 75-85% of the neurons in this area. In contrast,
354 inhibitory GABAergic interneurons comprise 15-25% of the local neurons ([Santana et al., 2004](#);
355 [Gabbott et al., 2005](#)). Previous studies have shown that PL glutamatergic
356 (PL^{GLUT}) neurons are necessary for the retrieval of conditioned threat responses ([Do-
357 Monte et al., 2015](#)), whereas PL GABAergic (PL^{GABA}) neurons are implicated in both the
358 encoding and the retrieval of threat associations by regulating the firing rate of PL^{GLUT}
359 neurons ([Courtin et al., 2014](#); [Cummings and Clem, 2020](#)). In addition, during foraging
360 in a safe context, food-associated cues activate both PL^{GLUT} and PL^{GABA} neurons
361 ([Burgos-Robles et al., 2013](#); [Gaykema et al., 2014](#)), and inactivation of PL^{GLUT} neurons
362 may increase or reduce conditioned food-seeking responses depending on the specific
363 downstream projections that are being modulated ([Otis et al., 2017](#)). While these
364 studies suggest a role for both PL^{GLUT} and PL^{GABA} neurons in the regulation of threat
365 and food-seeking responses in isolation, it remains unexplored how these two subsets
366 of PL neurons regulate the trade-off between seeking rewards and avoiding potential

367 threats during a conflict situation. To address this question, we combined single-unit
368 recordings with optogenetics to track the neuronal activity of photoidentified PL^{GLUT} and
369 PL^{GABA} neurons during the test session.

370 For photoidentification of PL^{GLUT} neurons, we injected into PL a viral vector (AAV-
371 CaMKII α -hChR2-(H134R)-eYFP) with a gene promoter (CaMKII α) that favors the
372 expression of the light-activated cation channel channelrhodopsin (ChR2) in PL^{GLUT}
373 neurons. This CaMKII α labeling approach has been successfully used in previous
374 studies ([Gradinaru et al., 2009](#); [Tye et al., 2011](#)) and was validated here for PL neurons
375 by showing a lack of immunocolabeling between the viral vector and the GABAergic
376 marker GAD67 (**Fig. 5A**). Rats expressing ChR2 selectively in PL^{GLUT} neurons were
377 implanted with an optrode into the same region for optogenetic-mediated identification
378 of PL^{GLUT} neurons at the end of the behavioral session (**Fig. 5B**). Among the recorded
379 PL cells, 36 out of 104 neurons (n = 5 rats) showed short-latency responses (< 6 ms)
380 and high spike reliability (Fano Factor ratio > 1) to laser illumination and were classified
381 as PL^{GLUT} neurons (**Fig. 5C-D** and Methods). The < 6 ms criterion was defined by using
382 the triangle method detection ([Zack et al., 1977](#)) to identify the cluster division in the
383 histogram distribution of response latencies (**Fig. 5C** and Methods). The < 6 ms criterion
384 was similar or stricter than the response latency criterion used in previous
385 photoidentification studies *in vivo* ([Lima et al., 2009](#); [Cohen et al., 2012](#); [Burgos-Robles](#)
386 [et al., 2017](#); [Allsop et al., 2018](#)). Photoactivation of PL^{GLUT} neurons can lead to indirect
387 activation of synaptically connected neurons in the same cortical region, but these
388 indirect responses to laser illumination take longer than 9 ms to occur ([Lima et al.,](#)
389 [2009](#)). For photoidentification of PL^{GABA} neurons, we injected into PL a viral vector

390 (AAV-mDlx-ChR2-mCherry) with a gene promoter (mDlx) that favors the expression of
391 ChR2 in PL^{GABA} neurons. This mDlx labeling approach has been successfully used in
392 previous studies ([Dimidschstein et al., 2016](#); [Sun et al., 2020](#)), and was validated here
393 for PL neurons by using two different methods: an immunohistochemical approach that
394 resulted in significant immunocolabeling between the viral vector and the GABAergic
395 marker GAD67 (**Fig. 5E**), and an *in situ* hybridization approach which confirmed that
396 ~88% of the cells labeled with the viral vector also expressed the GABAergic marker
397 vGAT (**Supplementary Fig. 7A-B**). Rats expressing ChR2 selectively in PL^{GABA}
398 neurons were implanted with an optrode into the same region for optogenetic-mediated
399 identification of PL^{GABA} neurons at the end of the behavioral session (**Fig. 5F**). Among
400 the recorded PL cells, 69 out of 338 neurons (n = 19 rats) showed short-latency
401 responses (< 6 ms) and high spike reliability (Fano Factor ratio > 1) to laser illumination
402 and were classified as PL^{GABA} neurons (**Fig. 5G-H and Methods**).

403 After separating the photoidentified cells into PL^{GLUT} and PL^{GABA} neurons, we
404 aligned their activities to the onset of the food cues and compared changes in firing
405 rates from the reward to the conflict phase in *Pressers* (**Fig. 5I**). We observed that the
406 proportions of excitatory and inhibitory food cue responses for PL^{GLUT} and PL^{GABA}
407 neurons were similar during the reward and the conflict phases (**Fig. 5J-K**, Fisher Exact
408 Test, all p's > 0.05). Next, we analyzed the spontaneous activity of PL^{GLUT} and PL^{GABA}
409 neurons and compared changes in their firing rates across the different phases of the
410 test session (**Fig. 5L**). We found that the average firing rate of PL^{GLUT} neurons remained
411 the same across the different phases of the test (~5 Hz; **Fig. 5M**, One-way repeated
412 measures ANOVA, $F_{(2.03, 69.02)} = 1.204$, p = 0.306), with most of the cells (57%) changing

413 their activities in more than one session (**Fig. 5N**). An average firing rate analysis
414 across phases demonstrated that the activity of PL^{GLUT} neurons didn't change
415 significantly from the reward to the odor phase (Fisher Exact Test, all p's > 0.05), but
416 was inhibited from the odor to the conflict phase when *Pressers* resumed searching for
417 food (**Fig. 5O**, Fisher Exact Test, odor vs conflict, p = 0.0046). Similar to PL^{GLUT}
418 neurons, the average firing rate of PL^{GABA} neurons also remained the same across the
419 different phases of the test (~8 Hz, **Fig. 5P**, One-way repeated measures ANOVA,
420 $F_{(1.164, 79.17)} = 0.013$, p = 0.935), with most of the cells (62%) changing their activities in
421 more than one session (**Fig. 5Q**). However, in contrast to PL^{GLUT} neurons, a group
422 analysis of the firing rates of PL^{GABA} neurons did not reveal significant differences
423 across the phases (**Fig. 5R**, Fisher Exact Test, all p's > 0.05). Because PL is comprised
424 of different subpopulations of interneurons that inhibit each other during food seeking or
425 defensive responses ([Gaykema et al., 2014](#); [Cummings and Clem, 2020](#)), we cannot
426 rule out the possibility that distinct subsets of PL^{GABA} neurons were preferentially
427 recruited during each one of the phases.

428 To evaluate how the spontaneous activity of the same PL neurons changed
429 during the test session, we tracked the firing rate of PL^{GLUT} and PL^{GABA} neurons across
430 the different phases. We found that all PL^{GLUT} neurons that were either excited or
431 inhibited during the reward phase responded in opposite direction or did not change
432 their activities during the odor phase (**Supplementary Figure 8A-B**), suggesting the
433 existence of distinct subpopulations of PL^{GLUT} neurons that encode reward and threat-
434 related information differently in our task. In contrast, no significant differences in the
435 proportions of excitation and inhibition were observed in PL^{GABA} neurons during the

436 transition from reward to odor phase nor during the transition from odor to conflict phase
437 for both subsets of PL neurons (**Supplementary Figure 8C-F**). Furthermore, both
438 PL^{GLUT} and PL^{GABA} neurons showed the same proportion of excitatory and inhibitory
439 responses before or after the onset of freezing, avoidance, or risk-assessment
440 behaviors (**Supplementary Figure 9A-F**, Fisher Exact Test, all p's > 0.05). These
441 results indicate that both glutamatergic and GABAergic neurons in PL may contribute to
442 the expression of distinct defensive responses during conflict. Together, our data
443 suggest that a significant proportion of PL^{GLUT} neurons are inhibited when rat's behavior
444 transitions from increased defensive responses during the conditioned odor phase to
445 increased food-seeking responses during the conflict phase.

446

447 **Photoactivation of PL^{GLUT}, but not PL^{GABA} neurons, suppresses reward-seeking**
448 **responses.**

449 To further establish whether changes in the activity of PL neurons can alter cue-
450 triggered food-seeking responses, we used an optogenetic approach to selectively
451 activate either PL^{GLUT} or PL^{GABA} neurons during a cued food-seeking test in a neutral
452 context. We initially infused either the viral vector AAV-CaMKII α -ChR2-eYFP (**Fig. 6A**)
453 or AAV-mDlx-ChR2-mCherry (**Fig. 6E**) into PL and implanted an optrode into the same
454 region to examine how photoactivation of PL^{GLUT} or PL^{GABA} neurons change local
455 activity. Laser illumination of PL^{GLUT} somata increased the firing rate of most responsive
456 PL neurons (9 out of 20 neurons, 45%), with some neurons showing reduced activity (6
457 out of 20 neurons, 30%, **Fig. 6B-D**). Neurons that increased their activities showed
458 shorter response latencies (3.31 ± 1.03 ms) compared to neurons that reduced their

459 activities (21.0 ± 3.74 ms) when analyzed in short bins of 1 ms, suggesting direct
460 responses (i.e., opsin-mediated) versus indirect responses (i.e., multi-synaptic),
461 respectively. Conversely, although some PL^{GABA} neurons showed increased activity
462 right after the laser onset (revealed by short bins of 1 ms, as shown in **Fig. 5E-H**),
463 illumination of PL^{GABA} somata reduced the firing rate of all responsive PL neurons when
464 analyzing the entire duration of the train (16 out of 22 neurons, 73%; **Fig. 6F-H**),
465 indicating a suppression in local activity.

466 After investigating the local effects of photoactivating either PL^{GLUT} and PL^{GABA}
467 neurons, we infused another set of animals with the same viral vectors in PL and
468 implanted bilateral optical fibers into the same region to manipulate PL activity during
469 the cued food-seeking test (**Fig. 6I-J**). Rats expressing only eYFP in PL were used to
470 control for any nonspecific effects of viral transduction or laser heating. To assess the
471 effects of PL photoactivation on lever presses, we alternated two trials of food cues with
472 the laser on vs. laser off conditions in a total of 12 trials (**Fig. 6K-L**). Photoactivation of
473 PL^{GLUT} (CaMKII-ChR2), but not PL^{GABA} (mDlx-ChR2) neurons, reduced the frequency of
474 lever presses (**Fig. 6M**, Two-way Repeated measures ANOVA, $F_{(10,180)} = 7.009$, $p <$
475 0.001 ; Bonferroni post-hoc, CaMKII-ChR2 vs. Control, all laser on periods - $p <$ 0.001 ,
476 mDlx-ChR2 vs. Control, all laser on periods - $p >$ 0.05) and increased the latency for
477 the first press after the cue onset (**Fig. 6N**, $F_{(10,180)} = 9.931$, $p <$ 0.001 ; Bonferroni post-
478 hoc, CaMKII-ChR2 vs. Control, all laser on periods - $p <$ 0.001 , mDlx-ChR2 vs. Control,
479 all laser on periods - $p >$ 0.05), when compared to control group. Photoactivation of
480 either PL^{GLUT} or PL^{GABA} neurons did not induce freezing behavior (**Fig. 6O**, $F_{(10,180)} =$
481 1.124 , $p = 0.346$). These results are consistent with our electrophysiological recordings

482 in **Fig. 5O** showing that increased inhibition in the firing rate of PL^{GLUT} neurons
483 correlates with augmented reward-seeking responses during conflict. Overall, these
484 findings suggest that increasing the activity of PL^{GLUT} neurons is sufficient to suppress
485 cued reward-seeking responses in a neutral context.

486

487 **Photoinhibition of PL^{GLUT} neurons in *Non-pressers* reduces freezing responses**
488 **and increases food approaching during conflict.**

489 Our electrophysiological experiments in **Fig. 5O** demonstrate that PL^{GLUT}
490 neurons are inhibited when rats' behavior transitions from defensive responses in the
491 odor phase to food-seeking responses in the conflict phase. In addition, our
492 photoactivation experiments in **Fig. 6K-O** indicate that increasing the activity of PL^{GLUT}
493 neurons suppresses cued reward-seeking behavior in rats that are pressing a lever for
494 food. We therefore hypothesized that photoinhibition PL^{GLUT} neurons during conflict
495 would attenuate defensive behaviors and rescue food-seeking responses in *Non-*
496 *Pressers*. To test this hypothesis, we injected a group of rats with the viral vector AAV-
497 CaMKII α -eNpHR-eYFP (or AAV-CaMKII α -eYFP) into PL to express the inhibitory opsin
498 halorhodopsin (or eYFP control) selectively in PL^{GLUT} neurons (**Fig. 7A**). Rats were
499 initially exposed to a cued food-seeking test to assess the effects of photoinhibition of
500 PL^{GLUT} neurons on food-seeking responses in a neutral context. We observed that
501 photoinhibition of PL^{GLUT} neurons had no effect on lever pressing rate (Two-way
502 repeated measures ANOVA, $F_{(5,110)} = 1.336$, $p = 0.254$), latency to press the lever
503 ($F_{(5,110)} = 0.637$, $p = 0.671$) or freezing ($F_{(5,95)} = 1.395$, $p = 0.231$) responses before
504 threat conditioning (**Supplementary Fig. 10A-E**).

505 Animals were then threat conditioned as in **Fig. 1** and on the following day
506 exposed to the odor arena for a test session. During the conflict phase, the first pair of
507 food cues was used to classify the animals into *Pressers* and *Non-Pressers*, whereas
508 the subsequent pairs of food cues were alternated between laser on and laser off
509 conditions to assess the effects of illumination of PL^{GLUT} neurons on approach-
510 avoidance responses (**Fig. 7B-C**). Remarkably, photoinhibition of PL^{GLUT} neurons
511 (CaMKII-eNpHR, Shapiro-Wilk normality test, all p's < 0.05) in *Non-Pressers* reduced
512 the percentage of time rats spent freezing (**Fig. 7D**, Wilcoxon test, $W = -64$, laser off vs.
513 laser on, $p = 0.0020$, Mann-Whitney Test, $U = 18$ Control vs. CaMKII-eNpHR, $p = 0.319$)
514 and avoiding the odor area (**Fig. 7E**, Wilcoxon test, $W = -21$, laser off vs. laser on, $p =$
515 0.031 ; Mann-Whitney Test, $U = 19.5$ Control vs. CaMKII-eNpHR, $p = 0.365$), and
516 increased the percentage of time rats spent approaching the food area (**Fig 7F**,
517 Wilcoxon test, $W = 21$, laser off vs. laser on, $p = 0.031$; Mann-Whitney Test, $U = 17$
518 Control vs. CaMKII-eNpHR, $p = 0.221$) during the food cue presentation, when
519 compared to the eYFP-control group (Wilcoxon test, Freezing: $W = 3$, laser off vs. laser
520 on, $p = 0.812$; avoidance: $W = 3$, laser off vs. laser on, $p = 0.500$, time in food area: $W =$
521 -3 , laser off vs. laser on, $p = 0.500$). Despite the increase in food approaching behavior,
522 photoinhibition of the same cells had no effect on the percentage of rewarded lever
523 presses (**Fig. 7G**, Wilcoxon test, $W = 6$, laser off vs. laser on, $p = 0.250$; Mann-Whitney
524 Test, $U = 22.5$ Control vs. CaMKII-eNpHR, $p = 0.697$) or latency to press the lever (**Fig.**
525 **7H**, Wilcoxon test, $W = -10$, laser off vs. laser on, $p = 0.125$; Mann-Whitney Test, $U = 21$
526 Control vs. CaMKII-eNpHR, $p = 0.357$), when compared to the control group (Wilcoxon

527 test, rewarded lever presses: $W = -1$, laser off vs. laser on, $p > 0.999$; latency to press
528 the lever: $W = 1$, laser off vs. laser on, $p > 0.999$).

529 In another subset of *Non-Pressers* (**Fig. 7I-K**), photoactivation of PL^{GABA} neurons
530 (mDlx-ChR2, Shapiro-Wilk normality test, all p 's < 0.05) did not alter freezing (**Fig. 7L**,
531 Wilcoxon test, $W = 18$, laser off vs. laser on, $p = 0.156$; Mann-Whitney Test, $U = 14$
532 Control vs. mDlx-ChR2, $p > 0.999$), avoidance (**Fig. 7M**, Wilcoxon test, $W = 4$, laser off
533 vs. laser on, $p = 0.500$; Mann-Whitney Test, $U = 12$ Control vs. mDlx-ChR2, $p = 0.772$)
534 time in food area (**Fig. 7N**, Wilcoxon test, $W = -2$, laser off vs. laser on, $p = 0.750$;
535 Mann-Whitney Test, $U = 11$ Control vs. mDlx-ChR2, $p = 0.660$) rewarded lever presses
536 (**Fig. 7O**, Wilcoxon test, $W = 3$, laser off vs. laser on, $p = 0.500$; Mann-Whitney Test, U
537 $= 13.5$ Control vs. mDlx-ChR2, $p > 0.999$) and latency to press the lever (**Fig. 7P**,
538 Wilcoxon test, $W = -3$, laser off vs. laser on, $p = 0.500$; Mann-Whitney Test, $U = 10$
539 Control vs. mDlx-ChR2, $p = 0.490$), when compared to the control group (eYFP-control
540 virus, white bars, $n = 4$, Wilcoxon test, freezing: $W = -2$, laser off vs. laser on, $p = 0.875$;
541 avoidance, $W = 0$, $p > 0.999$, time in food area: $W = 3$, $p = 0.500$, rewarded lever
542 presses: $W = 1$, $p = 0.500$, latency to press the lever: all animals reached maximum
543 latency). Photoactivation of PL^{GABA} neurons in *Pressers* also did not affect defensive
544 responses and food seeking behavior during the conflict test (**Supplementary Fig. 11A-**
545 **H**, Repeated measures ANOVA, all p 's > 0.05). Taken together, these results
546 demonstrate that reduced activity in PL^{GLUT} neurons during conflict situations decreases
547 defensive responses and biases rats' behavior toward food seeking.

548

549

550 **DISCUSSION**

551 Using a novel approach-avoidance conflict test, we demonstrated that PL neurons
552 regulate reward-approach vs. threat-avoidance responses during situations of
553 uncertainty, when rats use previously associated memories to guide their decisions. We
554 found that increased risk-taking behavior in *Pressers* was associated with a larger
555 number of food-cue responses in PL neurons, which showed sustained excitatory
556 activity that persisted during the conflict phase, when compared to *Non-Pressers*. In
557 addition, PL^{GLUT} neurons showed reduced spontaneous activity during risky reward
558 seeking and photoactivation of these cells in a neutral context was sufficient to suppress
559 lever press responses. Accordingly, photoinhibition of PL^{GLUT} neurons at the onset of
560 the food cues in *Non-Pressers* reduced defensive responses and increased food-
561 approaching during the conflict phase, consistent with our observation that a small
562 fraction of PL neurons changed their activity at the onset of freezing, avoidance or risk-
563 assessment responses. Altogether, these results suggest that under memory-based
564 conflict situations, reduced or increased activity in PL^{GLUT} neurons can favor the
565 behavioral expression of food-approaching or threat-avoidance responses, respectively.

566 During our approach-avoidance conflict test, *Pressers* and *Non-Pressers* showed
567 similar levels of lever pressing before the conflict phase (e.g., cued food-seeking
568 training, threat conditioning, and reward phases). This observation suggests that these
569 two individual phenotypes most likely emerged during the test session and were
570 independent of prior differences in sucrose preference or food-seeking motivation.
571 Similarly, because both groups exhibited the same percentage of freezing to the shock-
572 paired odor during the olfactory threat conditioning session, the increased defensive

573 behaviors and the reduced food-seeking responses observed in *Non-Pressers* during
574 the test session were unlikely due to higher acquisition of conditioned threat responses.
575 Furthermore, other internal factors such as shock sensitivity or pain tolerance cannot be
576 accounted for the individual differences observed in our experiments because both
577 groups reacted equally to the unconditioned stimulus (i.e., velocity measured as
578 maximum speed after the footshocks) and, different from other conflict tasks using
579 footshocks as a punishment during the conflict test (Geller, 1960; Vogel et al., 1971;
580 Oberrauch et al., 2019), in our model rats were not exposed to footshocks during the
581 conflict phase. Therefore, the most plausible interpretation for the behavioral differences
582 observed in our task is that *Pressers* and *Non-Pressers* have allocated distinct
583 motivational significance to the food- or shock-paired cues during the test session.

584 Individual differences in risky decision making have also been reported in other
585 studies using rodent models of behavioral conflict involving footshock punishment
586 (Simon et al., 2009; Jean-Richard-Dit-Bressel et al., 2019; Bravo-Rivera et al., 2021),
587 reversal learning (Bari et al., 2010), or variations in reward probability (Ainslie, 1975; St
588 Onge and Floresco, 2009; Dellsu-Hagedorn et al., 2018), although the neural
589 mechanisms underlying such differences are less clear. Evidence indicates that some of
590 the neurobiological bases of individual variation in stimulus-reward response depend on
591 differences in dopamine levels in subcortical circuits (Tomie et al., 2000; Flagel et al.,
592 2007; Flagel et al., 2011), which are regulated by top-down mechanisms involving the
593 mPFC (Ferenczi et al., 2016; Haight et al., 2017; Serrano-Barroso et al., 2019).
594 Accordingly, our neural correlate analyses of risk-taking vs. risk-avoiding behaviors in
595 the PL subregion of the mPFC revealed some clear differences between the two

596 phenotypes, suggesting that PL neurons participate in behavioral selection when rats'
597 decision depends on the conflicting memories of reward and threat. Both *Pressers* and
598 *Non-Pressers* showed a reduction in the number and magnitude of food-cue responses
599 from reward to conflict phases, indicating that PL neurons can differentiate between
600 situations involving motivational conflict and those that do not.

601 One intriguing finding in our study was the observation that *Pressers* showed a
602 larger number of sustained excitatory food-cue responses during the conflict phase,
603 when compared to *Non-Pressers*. Because PL neurons are known for encoding the
604 value of reward-predictive cues ([Sharpe and Killcross, 2015](#); [Otis et al., 2017](#)), the
605 increase in the number and magnitude of food cue responses observed in *Pressers*
606 might result in a greater allocation of attention to reward cues, which would explain the
607 persistent reward-seeking responses observed in this group during motivational conflict.
608 In support of this interpretation, reward-paired cues can acquire motivational salience in
609 some subjects and become sufficient to elicit reward-seeking responses in both rodents
610 ([Robinson and Flagel, 2009](#); [Robinson et al., 2014](#)) and humans ([Smith et al., 2011](#);
611 [Jensen and Walter, 2014](#)). Consistently, *Pressers* also showed a larger number of food
612 cue responses in PL before the conflict phase (i.e., reward phase), although the
613 percentage of rewarded presses and the latency to press the lever during the reward
614 phase were similar between the two groups.

615 Another possible interpretation for the differences in food-cue responses in
616 *Pressers* and *Non-Pressers* is the reduced excitatory food cue responses in *Non-*
617 *Pressers*, which may be mediated by cue-evoked activity in inhibitory inputs to PL
618 during the conflict phase. While the source of this inhibition is unclear, a potential

619 candidate are GABAergic neurons in the ventral tegmental area (VTA^{GABA}), which
620 correspond to 35% of the cells in this region and send significant projections to PL
621 ([Nair-Roberts et al., 2008](#); [Breton et al., 2019](#)). Previous studies have shown that
622 VTA^{GABA} neurons change their firing rates in response to reward-predicting cues ([Cohen](#)
623 [et al., 2012](#)), and chemogenetic activation of these cells suppress the activity of local
624 dopaminergic neurons ([van Zessen et al., 2012](#)), reduces cue-evoked sucrose-seeking
625 responses ([Wakabayashi et al., 2019](#)), and induces conditioned place aversion in
626 rodents ([Tan et al., 2012](#)). Future studies need to determine whether this regulation of
627 rewarding and aversive responses by VTA^{GABA} neurons can also be attributed to their
628 long-range inhibitory projections to PL neurons, particularly during conflict situations.

629 Differences in risk-taking and risk-avoiding behaviors were also reflected on LFP
630 frequencies in PL neurons in the beginning of the test session, with *Pressers* and *Non-*
631 *Pressers* displaying increased power in the delta or theta bands, respectively. These
632 findings are in corroboration with previous studies showing that increased delta power
633 activity in the mPFC is associated with both reward seeking and preparatory attention
634 ([Horst and Laubach, 2013](#); [Totah et al., 2013](#); [Emmons et al., 2016](#)), whereas
635 augmented theta power in the mPFC or synchronized theta activity between mPFC and
636 BLA is correlated with the expression of avoidance responses or the consolidation of
637 threat memories, respectively ([Popa et al., 2010](#); [Padilla-Coreano et al., 2019](#)). More
638 specifically, increased synchrony between mPFC and BLA activity in the theta
639 frequency range has been reported for animals that successfully differentiate between
640 aversive and safe cues (or environments) during a differential threat conditioning task
641 (or an open field arena) ([Likhnik et al., 2014](#); [Stujenske et al., 2014](#)). In addition, prior

642 studies have shown that 4 Hz LFP oscillations in the mPFC and BLA were strongly
643 synchronized during conditioned freezing episodes ([Courtin et al., 2014](#); [Dejean et al.,](#)
644 [2016](#); [Karalis et al., 2016](#)), and these sustained 4 Hz oscillations in the mPFC were
645 independent of hippocampal low-theta oscillations, suggesting that they were internally
646 generated in the mPFC during the expression of freezing behavior ([Karalis et al., 2016](#)).
647 Consistent with these findings, in our study *Non-Pressers* showed increased theta
648 activity and marked 4 Hz oscillations in PL neurons, which were associated with better
649 discrimination between reward and threat cues and increased freezing responses
650 during the test session, when compared to *Pressers*.

651 Increased risk-taking behavior in *Pressers* was associated with a higher number
652 of PL^{GLUT} neurons showing reduced spontaneous activity during the conflict phase. In
653 contrast, risk-avoiding responses in *Non-Pressers* were associated with increased
654 spontaneous activity during conflict. While this set of results suggest that distinct
655 patterns of PL activity are associated with risk-taking or risk-avoiding behaviors in
656 conflict situations, our optogenetic manipulation provided a causal role for PL^{GLUT}
657 neurons in the regulation of approach-avoidance conflict. For instance, the reduction in
658 food-seeking responses during photoactivation of PL^{GLUT} neurons indicates that
659 increased activity in PL pyramidal cells is sufficient to recapitulate the reward-seeking
660 suppression observed during conflict. Our findings agree with previous studies showing
661 that increased activity in mPFC neurons, including PL, attenuates reward-seeking
662 responses in a neutral context ([Berglind et al., 2007](#); [Chen et al., 2013](#); [Ferenczi et al.,](#)
663 [2016](#); but see: [Warthen et al., 2016](#)), an effect that has been attributed, at least in part,
664 to downstream projections to the paraventricular nucleus of the thalamus (PVT) ([Otis et](#)

665 [al., 2017](#)). Notably, PVT neurons are necessary for the retrieval of both reward- and
666 threat-associated memories (for a review see: [Do Monte et al., 2016](#); [Millan et al., 2017](#);
667 [McGinty and Otis, 2020](#); [Penzo and Gao, 2021](#)), and activity in PVT neurons has
668 recently been shown to be associated with the regulation of approach-avoidance
669 responses during situations of conflict ([Choi and McNally, 2017](#); [Choi et al., 2019](#);
670 [Engelke et al., 2021](#)), suggesting a potential target by which PL glutamatergic neurons
671 may exert their effects.

672 Considering that *Pressers* showed a higher number of sustained excitatory food-
673 cue responses than *Non-Pressers*, it is counterintuitive that photoactivation of PL^{GLUT}
674 neurons during the food cue onset resulted in reduced food-seeking responses.
675 However, it is important to note that our optogenetic manipulation not only altered the
676 activity of food-cue responsive neurons, but mostly the global activity of other PL^{GLUT}
677 neurons. Thus, it is possible that increased activity in the firing rate of PL^{GLUT} neurons
678 may result in reduced signal-to-noise ratio during the food cue onset ([Kroener et al.,](#)
679 [2009](#); [McGinley et al., 2015](#)), and consequently decreased food-seeking responses. In
680 contrast, we speculate that by reducing their spontaneous firing rates during conflict
681 situations, PL^{GLUT} neurons become more likely to fire in response to food cues due to an
682 increase in the signal-to-noise ratio, thereby resulting in persistent reward-seeking
683 responses during the conflict phase as we propose in our schematic in Fig. 8.

684 Additionally, our findings showing that inactivation of PL^{GLUT} neurons increases
685 food-approaching responses in *Non-Pressers* suggest that PL activity is indispensable
686 to inhibit reward pursuit in the presence of threat-associated cues. The lack of effects on
687 lever pressing indicate that other parallel brain regions may be modulating the

688 suppression of operant lever-press responses during conflict. Alternatively,
689 photoinhibition of PL^{GLUT} neurons was not large enough to produce a more global effect
690 on risky behavior (i.e., completely restore lever presses). Collectively, these results add
691 to a growing literature indicating that PL neurons are necessary to guide appropriate
692 food-seeking behavior in tasks that rely on discrimination among environmental cues
693 (Marquis et al., 2007; Sangha et al., 2014; Moorman and Aston-Jones, 2015) or
694 decision-making tasks involving risk of punishment in which animals need to: i) adapt
695 choice behavior during shifts in risk contingencies (Orsini et al., 2018), ii) regulate
696 behavioral flexibility (Radke et al., 2015; Capuzzo and Floresco, 2020), or iii) suppress
697 reward seeking in response to conditioned aversive stimuli (Kim et al., 2017; Piantadosi
698 et al., 2020). Moreover, our results are in accordance with previous findings
699 demonstrating that inactivation of PL neurons, or their inputs from BLA, increases risk-
700 taking behavior in a conflict task in which rats needed to refrain from consuming
701 sucrose to avoid a footshock (Burgos-Robles et al., 2017; Verharen et al., 2019).

702 Previous studies have shown that PL neurons fire in response to shock-paired
703 cues and such activity is highly correlated with the expression of freezing responses
704 (Burgos-Robles et al., 2009; Sotres-Bayon et al., 2012; Kim et al., 2013; Courtin et al.,
705 2014). Adding to these findings, our recordings demonstrated that the activity of a small
706 number of PL neurons changed immediately before or after the onset of freezing
707 responses, with the same proportion of freezing-responsive cells being classified as
708 PL^{GLUT} or PL^{GABA} neurons (~6-14%). At first sight, the lack of effects on freezing
709 behavior following optogenetic activation of PL^{GLUT} neurons seems at odds with our
710 recordings. It also seems to disagree with previous studies showing that electrical

711 stimulation or optogenetic induction of 4Hz oscillations in PL increases conditioned
712 freezing responses ([Vidal-Gonzalez et al., 2006](#); [Courtin et al., 2014](#)) by synchronizing
713 the neural activity between PL and BLA regions ([Karalis et al., 2016](#)). However, one
714 important difference between our study and others is that photoactivation of PL^{GLUT}
715 neurons in our experiments was performed in naïve rats, in the absence of shock-paired
716 cues. Thus, the increased freezing responses following PL activation reported in
717 previous studies appear to be dependent on the preexistence of a conditioned threat
718 memory.

719 Overall, our results outline the neural correlates of risk-taking and risk-avoiding
720 behaviors in PL and reveal an important role for PL^{GLUT} neurons in coordinating
721 memory-based risky decision-making during conflict situations. Further studies will
722 focus on identifying the PL downstream/upstream circuits that regulate reward-
723 approaching and threat-avoidance responses, as well as the potential genetic and
724 epigenetic factors that could contribute to the observed behavioral phenotypes.
725 Elucidating the underlying mechanisms that mediate risk-taking vs. risk-avoiding
726 responses during situations of uncertainty may help to provide understanding of
727 response selection and adaptive behaviors, and may have clinical relevance to many
728 psychiatric disorders ([Aupperle and Paulus, 2010](#); [Kirlic et al., 2017](#)). Whereas
729 persistent avoidance of presumed threats is the cardinal symptom of anxiety disorders
730 ([Treanor and Barry, 2017](#)), seeking reward despite negative consequences is a
731 hallmark of both eating and substance use disorders in humans ([Volkow et al., 2012](#)).

732

733

734 **ACKNOWLEDGEMENTS**

735 We thank Dr. Roger Janz for helping us with the packaging of the AAV-mDLX-ChR2-
736 mCherry viral construct, Rya Albert and Sharon Gordon for their technical assistance,
737 and Dr. Robson Scheffer-Teixeira for his support with the statistical analyses. We also
738 thank current and former members of the Do Monte and Quirk Labs for their valuable
739 comments on the manuscript, and the Mind the Graph team for creating the schematic
740 drawings presented in the manuscript. This work was supported by NIH grants R00-
741 MH105549 and R01-MH120136, a Brain & Behavior Research Foundation grant
742 (NARSAD Young Investigator), and a Rising STARs Award from UT System to F.H.D-
743 M.

744

745 **Author contributions**

746 J.A.F-L., D.S.E., and G.A.M. performed the behaviors, optogenetics, and single-unit
747 recordings. D.S.E. carried out the immunohistochemical and *in situ* hybridization
748 studies. A.G. wrote and validated the DeepLabCut and the Python codes for behavioral
749 analyses. M. N. R. helped training the animals and performing the histological analyses.
750 J.A.F-L. wrote the MATLAB and Python codes for single-unit recording analyses. Both
751 J.A.F-L. and F.H.D-M. analyzed the single-unit recording and behavioral data. D.S.E.
752 performed the statistical analyses. All the authors helped to design the study and
753 interpret the data. J.A.F-L., D.S.E and F.H.D-M. prepared the manuscript with
754 comments from all the co-authors.

755

756 **Competing interests**

757 The authors declare no competing interests.

758

759 **Correspondence and requests for materials** should be addressed to F.H.D-M.

760

761 **METHODS**

762 **Animals.** All experimental procedures were approved by the Center for Laboratory
763 Animal Medicine and Care of The University of Texas Health Science Center at
764 Houston. The National Institutes of Health guidelines for the care and use of laboratory
765 animals were strictly followed to minimize any potential discomfort and suffering of the
766 animals. Male Long-Evans hooded adult rats (Charles Rivers Laboratories) with 3-5
767 months of age and weighing 300-450 g at the time of the experiment were used. Rats
768 were single-housed and after a 3-day acclimation period handled and trained to press a
769 lever for sucrose as described below. Animals were kept in a 12-hour light/12-hour dark
770 cycle (light from 7:00 to 19:00) and maintained on a restricted diet of 18 g of standard
771 laboratory rat chow provided daily at the end of experimentation. Animals were given *ad*
772 *libitum* access to water. Animals' weights were monitored weekly to ensure all animals
773 maintained their weight under food restriction. During pre- and post- surgery phases,
774 animals were given *ad libitum* access to food for a total of 7 days.

775 **Surgeries.** Rats were anaesthetized with 5% isoflurane in an induction chamber.
776 Animals were positioned in a stereotaxic frame (Kopf Instruments) and anesthesia was
777 maintained with 2.5% isoflurane delivered through a facemask. A heating pad was
778 positioned below the body of the animal and both temperature and respiration were
779 monitored during the entire surgery. Veterinary lubricant ointment was applied on the

780 eyes to avoid dryness during the surgery. Animals received a subcutaneous injection of
781 the local anesthetic bupivacaine (0.25%, 0.3 ml) at the incision site. Iodine and ethanol
782 (70%) were alternately applied for asepsis of the incision site. The surgery procedures
783 varied according to the type of implantation/injection (see below). For injection-only
784 surgeries, the incision was stitched after the injection by using surgical suture (Nylon, 3-
785 0). For implantation surgeries, the implants were fixed to the skull using C&B metabond
786 (Parkell), ortho acrylic cement, and four to six anchoring screws. After surgery, animals
787 received a subcutaneous injection of meloxicam (1 mg/Kg) and a topical triple antibiotic
788 was applied to the incision area.

789 **Viral vector injection.** Viral injections were performed using a microsyringe (SGE, 0.5
790 μ l) with an injection rate of 0.04 μ l/min plus an additional waiting time of 12 min to avoid
791 back-flow. The adeno-associated virus (AAV) was bilaterally injected at a volume of 0.4
792 μ l per side. The AAV-CaMKII α -eNpHR-eYFP vector was used to inhibit glutamatergic
793 neurons, whereas AAV-mDlx-ChR2-mCherry or AAV-CaMKII α -ChR2-eYFP vectors
794 were used to activate either GABAergic or glutamatergic neurons, respectively. The use
795 of mDlx or CaMKII α promoters enabled transgene expression favoring either
796 GABAergic or glutamatergic neurons, as previously shown ([Gradinaru et al., 2009](#); [Tye](#)
797 [et al., 2011](#); [Dimidschstein et al., 2016](#); [Sun et al., 2020](#)) and was confirmed by our
798 immunohistochemical and RNAscope assessment (**Supplementary Fig. 7**). The viral
799 construct AAV-CaMKII α -eYFP was used to control for any nonspecific effects of viral
800 infection or laser heating. All plasmid or viral vectors were obtained from Addgene or
801 University of North Carolina Viral Vector Core. For implantation of optrodes, the
802 following coordinates from bregma were used for virus injection: PL, +2.7 mm AP, \pm 0.7

803 mm ML, -3.8 mm DV at a 0° angle. For PL soma illumination, an optical fiber (0.39 NA,
804 200 nm core, Inper) was implanted in each hemisphere targeting PL neurons using the
805 following coordinates from bregma: +2.7 mm AP; ±1.5 mm ML; -4.0 mm DV at a 15°
806 angle.

807

808 **Single-unit electrodes.** An array of 16 or 32 microwires was unilaterally implanted
809 targeting the PL using the following coordinates from bregma: +2.7 mm AP, ±0.8 mm
810 ML, -3.9 mm DV. Three different electrode configurations were used: i) 32-channel
811 silicon probes (Buzsaki32-CM32 or A1x32-5mm-25-177-CM32, Neuro Nexus
812 Technologies, USA), ii) Micro-Wire Arrays (MWA) of 16 or 32 channels (Bio-Signal
813 Technologies Ltd, USA); or iii) custom designed electrodes with 2×8 grid with 150 μm of
814 space between wires, 200 μ of space between rows, with 35 μm diameter wires
815 (Innovative Neurophysiology Inc., USA). For photoidentification of GABAergic or
816 glutamatergic neurons, a Hermes 32 channels optrode array was used (200 nm core,
817 Bio-Signal Technologies Ltd). Optrodes were unilaterally implanted at the same
818 coordinates described above after the infusion of 0.6 μl of AAV-mDlx-ChR2-mCherry or
819 AAV-CaMKIIα-ChR2-eYFP vectors. In all cases, the ground wire was wrapped around a
820 grounding screw previously anchored into the skull. Two insulated metal hooks were
821 implanted bilaterally into the cement to allow firmly attachment of the array connector to
822 the cable during recording.

823 **Odor preparation.** A 99% amyl acetate solution (Sigma Aldrich) was diluted in
824 propylene glycol (Bluewater Chemgroup, Inc) to a 10% solution and presented to the
825 rats during the different stages and phases of the olfactory threat conditioning test. A

826 customized olfactometer (Med Associates) was used to control the flow of air into the
827 animal's chamber. Before being mixed with the 10% amyl acetate solution, the air was
828 passed through a desiccant and a charcoal filter to remove any moisture and odors, and
829 was finally rehydrated with distilled water before being delivered into the chamber
830 through a thermoplastic PVC-based tube (Tygon) attached to an odor port located in the
831 odor area.

832 **Behavioral Tasks**

833 Lever-press training. Rats were placed in a plexiglass, standard operant box (34 cm
834 high x 25 cm wide x 23 cm deep, Med Associates), and trained to press a lever for
835 sucrose on a fixed ratio of one pellet for each press. Next, animals were trained in a
836 variable interval schedule of reinforcement that was gradually reduced across the days
837 (one pellet every 15 s, 30 s, or 60 s) until the animals reached a minimum criterion of 10
838 presses/min. All sessions lasted 30 min and were performed on consecutive days.
839 Sucrose pellet delivery, variable intervals, and session duration were controlled by an
840 automated system (ANY-maze, Stoelting). Lever-press training lasted approximately
841 one week, after which animals were assigned to surgery or cued food-seeking training.
842 A small number of rats failed to reach the lever press criteria and were excluded from
843 the experiments (< 3%).

844 Cued food-seeking training. Rats previously trained to press a lever for sucrose were
845 trained to learn that each lever press in the presence of an audiovisual cue (tone: 3
846 KHz, 75 dB; light: yellow, 2.8 W; 30 s duration) resulted in the delivery of a sucrose
847 pellet into a nearby dish. Reward cue conditioning also took place in the standard
848 operant boxes. While the light cue helps to direct the animals toward the lever during

849 the beginning of the training phase, the tone assures that the animals will not miss the
850 presentation during the trial and provides the temporal precision required for single-unit
851 recordings. After ~4 consecutive days of training (24 trials per day, pseudorandom
852 intertrial interval of ~120 s, 60 min session), rats learned to discriminate the food-
853 associated cue as indicated by a significant increase in press rate during the presence
854 of the audiovisual cues, when compared to the 30 s immediately before the cue onset
855 (cue-off, see **Supplementary Fig. 1A**). The cued food-seeking training was completed
856 when animals reached 50% of discriminability index (presses during cue-on period
857 minus presses during cue-off period divided by the total number of presses). After the
858 cued food-seeking training was completed, rats with single-unit electrodes were
859 exposed to an additional training session in which the audiovisual cue ceased
860 immediately after the animals pressed the lever and a single sucrose pellet was
861 delivered into the dish. This extra training reduced the rat's response to a single press
862 and dish entry per cue, thereby enabling us to correlate each food-seeking event with
863 the neuronal firing rate by avoiding overlapping between consecutive events (e.g., lever
864 presses). The single-pellet training took place in the same plexiglass rectangular arena
865 subsequently used for the odor test (40 cm high x 60 cm wide x 26 cm deep, Med
866 Associates, see schematic in **Fig. 1A right**). The arena consisted of a hidden area (40
867 cm high x 20 cm wide x 26 cm deep) separated from an open area by a plexiglass
868 division. An 8-cm slot located in the center of the division enabled the animal to
869 transition between both sides of the arena. For behavioral quantification, the open area
870 was subdivided into a center area and a food area (40 cm high x 12 cm wide x 26 cm

871 deep), the latter containing a lever, a dish, and an external feeder similar to the food-
872 seeking operant box.

873 Habituation day. Animals were placed in the odor arena and exposed to 12 audiovisual
874 cues (30 s duration, pseudorandom inter-trial intervals of between 25-40 s) followed by
875 10 min of presentation to the neutral odor alone (10% amyl acetate) and an additional
876 12 audiovisual cues similar to the first cues but in the presence of the neutral odor
877 delivered in the food area of the arena. Each lever press in the presence of the
878 audiovisual cue resulted in the delivery of a sucrose pellet into the dish, and the
879 audiovisual cue ceased immediately after the animal pressed the lever.

880 Threat conditioning day. One day after the habituation day, rats were placed in a
881 plexiglass, standard operant box similar to the cued food-seeking training box, but with
882 the grid floor previously attached to a shock generator system. Rats were habituated to
883 one non-reinforced odor presentation (10% amyl acetate, 30 s duration) followed by five
884 odor presentations that coterminated with a foot shock (0.7 mA, 1 s duration, 258-318 s
885 inter-trial intervals). An olfactometer system was used to deliver the odor into the box
886 (see odor preparation session above), whereas an exhaustor system was used to
887 remove it during the intertrial intervals. Between each odor presentation, audiovisual
888 cues (30 s duration) signaling the availability of sucrose were presented to the animals.
889 Each lever press during the audiovisual cues resulted in the delivery of a sucrose pellet
890 into the dish. Shock grids and floor trays were cleaned with 70% ethanol between each
891 rat. No rats were excluded from the analyses due to distinct levels of freezing following
892 the threat conditioning session.

893 Test day. One day after the threat conditioning session, rats were returned to the same
894 arena used during the habituation and exposed to the exact same protocol. The first
895 phase of the test session was called *reward phase* (12 min) and the animals were
896 exposed to 12 food cues. The second phase was called *odor phase* and the animals
897 were exposed to 10 min of conditioned odor (10% amyl acetate) alone. The last phase
898 was called *conflict phase* (12 min) and the animals were exposed to 12 food cues in the
899 presence of the conditioned odor. An odor dispersion sensor (200B miniPID, Aurora
900 Scientific) revealed that the odor took approximately 2.21 ± 0.28 s to reach detectable
901 concentrations (56 particles per billion; Punter, 1983) in the arena after the olfactometer
902 onset, and approximately 19.59 ± 0.97 s to be completely removed from the arena after
903 the olfactometer offset and concomitant activation of the exhaustor fan. Due to the low
904 temporal resolution to control the delivery of the odor in the arena, the odor was
905 maintained constant during the entire duration of the odor and conflict phases. In order
906 to press the lever for sucrose during the conflict phase, rats had to approach the
907 conditioned odor presented in the food area. After the end of the conflict phase, the
908 odor was extracted from the arena with the exhaustor fan and the floor and walls of the
909 arena were cleaned thoroughly with 70% ethanol solution.

910 **Behavioral tracking.** Both the standard operant boxes and the testing arenas were
911 equipped with video cameras and a behavior tracking software (ANY-maze, Stoelting)
912 which were used to record the animal's behavior and control the delivery of sucrose,
913 foot shock, tone, light and odor in the apparatuses. Avoidance responses were
914 characterized by the time spent in the hidden area of the arena. Freezing responses
915 were characterized by the complete absence of movements except those needed for

916 respiration. Risk-assessment responses were characterized by a body stretching
917 movement to peep out toward the food area while in the hidden area and were used as
918 a measure of risk-assessment behavior ([Blanchard et al., 2011](#)).

919 For single-unit recording analyses, the detection of freezing, avoidance and risk
920 assessment behaviors were performed using the open source tool DeepLabCut, a
921 machine learning software that tracks complex patterns of behavior from videos ([Mathis
922 et al., 2018](#)). After a video has been analyzed, the data was saved to a .csv file that
923 contained the x and y location of each rat's body part in pixels, as well as the analysis of
924 the expected accuracy (i.e., likelihood) of the tracked positions across time. After
925 DeepLabCut has calculated the positions and the likelihood, we used three different
926 Python codes to identify each one of the three behaviors. For freezing behavior, the
927 code used DeepLabCut's position data and determined if the rat was still for more than
928 500 ms. The animal was considered to be still if the position in question was within 1.05
929 pixels of each other. For avoidance behavior, the code used DeepLabCut's position
930 data to determine the location of the rat in the arena and based on the center of its head
931 to identify when the animals entered the hidden area of the arena. Finally, for risk
932 assessment behavior, the code used DeepLabCut's position data to identify the nose,
933 ears, center of the head, and spine to determine whether the rat was located in the
934 hidden area of the arena with its body stretched and the head looking through the open
935 division of the apparatus. Each of these codes generated a .xlsx file that contained the
936 onset and the total duration of each behavioral episode (see single-unit analyses
937 section for more details).

938 **Optogenetic stimulation during behavior.** Bilateral optical cables (200 μm core, 0.37
939 NA, 2.5 mm ceramic ferrule, Inper) were connected to a blue laser (diode-pumped solid-
940 state, 473 nm, 150 mW output, OptoEngine) or a yellow laser (diode-pumped solid-
941 state, 593.5 nm, 300 mW output, OptoEngine) by using a patch cord (200 μm , 0.39 NA,
942 FC/PC connector, Inper) through a dual rotary joint (200 μm core, Doric lenses). During
943 the stimulation, the optical cables were coupled to the previously implanted optical
944 fibers by using a ceramic sleeve (2.5 mm, Precision Fiber Products). An optogenetic
945 interface (Ami-2, Stoelting) and an electrical stimulator (Master 9, A.M.P. Instruments)
946 were used to control the onset of the laser, pulse width, train duration, and frequency.
947 The power density estimated at the tip of the optical fiber was 7-10 mW for illumination
948 of PL somata (PM-100D, Power Energy Meter, Thor Labs).

949 **Single-unit recording.** A 64-channels neuronal data acquisition system (Omniplex,
950 Plexon) integrated with a high-resolution video-tracking system (Cineplex, Plexon) was
951 used for electrophysiological recordings from freely behaving animals. Both videos and
952 neuronal recordings were combined within the same file, thereby facilitating the
953 correlation of behavior with neuronal activity. An electrical isolation, Faraday cage was
954 made and connected to the grounding port of the data acquisition system. The system
955 was connected to the head-mounted electrode/optrode by using a digital headstage
956 cable (32 channels, Plexon), a motorized carrousel commutator (Plexon), and a digital
957 headstage processor (Plexon). Rats were habituated to the headstage cable daily for
958 approximately one week before the beginning of the experiments. Extracellular
959 waveforms exceeding a voltage threshold were band-pass filtered (500 - 5,000 Hz),
960 digitized at 40 KHz, and stored onto disk. Automated processing was performed using a

961 valley-seeking scan algorithm and then visually evaluated using sort quality metrics
962 (Offline Sorter, Plexon, see single-unit analyses section below).

963 **Photoidentification of PL neurons during recordings.** During neuronal
964 photoidentification, we recorded from rats expressing channelrhodopsin (ChR2) in PL
965 neurons previously implanted with an optrode in the same region. An optical cable
966 connected to a blue laser was attached to the headstage cable and coupled to the
967 previously implanted optical fiber by using a ceramic sleeve. At the end of the
968 behavioral session, 10 trains of 10-s blue laser pulses (5 ms pulse width, 5 Hz) were
969 delivered by a Master-9 programmable pulse stimulator, which also sent flags to the
970 data acquisition system to mark the time of the laser events.

971 Neurons were considered to be responsive to photoactivation if they showed a
972 significant increase in firing rate above baseline (20 ms, Z-score > 3.29, $p < 0.001$) and
973 higher reliability within the 6 ms after laser, similar to previous studies ([Lima et al., 2009](#);
974 [Pi et al., 2013](#); [Burgos-Robles et al., 2017](#); [Engelke et al., 2021](#)). To identify the
975 threshold separation for the frequency distribution of response latencies to laser
976 illumination, we implemented the Triangle Method detection ([Zack et al., 1977](#)). This
977 calculation is particularly effective for left-skewed distributions as in our sample. We
978 considered bins with response latency values from 0 to 12 ms and excluded those with
979 larger values as they would most likely reflect indirect stimulation via collateral activity.
980 We computed the distance normal to the line along with the minimum and maximum
981 values in the histogram. The threshold was defined as the maximum distance between
982 the histogram and the line (i.e. a normalized level within 0 and 1), which in our analysis
983 resulted in 5.8 ms (rounded to 6 ms bin). In addition, to measure the reliability of neural

984 responses to photoactivation, we calculated the Fano Factor (FF), defined as the
985 variance-to-mean ratio of spike counts (Churchland et al., 2011), to characterize the
986 variability of neuronal responses 6 ms before (FF before) and 6 ms after (FF after) the
987 laser pulses for each train of illumination (10 trains of 50 laser pulses, 200 ms pulse
988 interval). When the variance in the counts equals the mean count, FF was equal to 1.
989 Afterwards, we computed the 'overall FF ratio' between the 'FF after' divided by the 'FF
990 before' to compute the reliability of each cell to the laser onsets. Only neurons showing
991 an overall FF higher than 1, which indicates reliable responses to laser illumination
992 compared to baseline, were included as photoidentified cells.

993 A small number of laser-generated photoelectric artifacts (~10% of the channels
994 in less than 10% of the rats) were observed during the photoactivation. However, they
995 were easily distinguished from the action potentials by their descending voltage signals
996 of high amplitude, pulse shapes distinct from the regular waveforms, isolated spatial
997 distribution in the principal component analyses, and occurrence restricted to the period
998 of laser activation, which resulted in lack of activity during the behavioral session.

999 **Optogenetic manipulation of PL neurons during behavior.** During the cued food-
1000 seeking test, rats expressing ChR2 or eNpHR in PL were bilaterally illuminated in the
1001 same region by using a blue (5 ms pulse width, 5 Hz for CaMKII α or 20 Hz for mDlx) or
1002 a yellow laser (constant illumination), respectively. The laser was activated at cue onset
1003 and persisted throughout the entire 30 s of the audiovisual cue presentation. Rats were
1004 exposed to two consecutive cues with laser off followed by two consecutive cues with
1005 laser on in a total of 12 cues (pseudorandom inter-trial intervals of between 25-40 s). To
1006 assess the effects of PL illumination on rat's defensive behavior, PL neurons of rats

1007 expressing ChR2 or eNpHR were bilaterally illuminated during 6 distinct epochs of 30 s
1008 during the *odor phase* by using a blue (5 ms pulse width, 20 Hz) or a yellow laser
1009 (constant illumination), respectively. To assess the effects of PL illumination on food-
1010 seeking responses during the conflict phase, rats were exposed to two consecutive
1011 cues with laser off followed by two consecutive cues with laser on in a total of 12 cues
1012 (pseudorandom inter-trial intervals of between 25-40 s). The laser was activated at cue
1013 onset and persisted on until the animal pressed the bar or the 30 s of the audiovisual
1014 cue was completed.

1015 **Histology.** Animals were transcardially perfused with KPBS followed by 10% buffered
1016 formalin. Brains were processed for histology as previously described ([Do-Monte et al.,](#)
1017 [2013](#)). At the end of the recording sessions, a micro-lesion was made by passing
1018 anodal current (0.3 mA for 15 s) through the active wires to deposit iron in the tissue.
1019 After perfusion, brains were extracted from the skull and stored in a 30% sucrose/ 6%
1020 ferrocyanide solution to stain the iron deposits. Only rats with the presence of eYFP or
1021 mCherry labeling and the track of the electrode wires or optical fiber tips located
1022 exclusively in PL were included in the statistical analyses.

1023 **Immunohistochemistry.** Rats previously infused with AAV-mDlx-ChR2-mCherry or
1024 AAV-CaMKII α -ChR2-eYFP were transcardially perfused with 300 ml of KPBS followed
1025 by 500 ml of 4% paraformaldehyde. Brains were removed from the skull, transferred to
1026 a 20% sucrose solution in KPBS for 24 h, and stored in a 30% sucrose solution in KPBS
1027 for another 24 h. Next, coronal PL sections (40 μ m thick) were cut in a cryostat (CM
1028 1860, Leica), blocked in 20% normal goat serum and 0.3% Triton X-100 in KPBS at
1029 room temperature for 1 h. For identification of GABAergic neurons, PL sections were

1030 incubated with anti-GAD67 serum raised in rabbit (1:400; Millipore-Sigma) at 4°C for 48
1031 h. After sections were washed in KPBS for 5 times, sections were incubated with a
1032 secondary anti-rabbit antibody (1:200, Alexa Fluor 488 or Alexa Fluor 594, Abcam) for 2
1033 h. Sections were washed with KPBS, mounted in Superfrost Plus slides, and
1034 coverslipped with anti-fading mounting medium (Vectashield, Vectorlabs). Images were
1035 generated by using a microscope (Nikon, Eclipse NiE Fully Motorized Upright
1036 Microscope) equipped with a fluorescent lamp (X-Cite, 120 LED) and a digital camera
1037 (Andor Zyla 4.2 PLUS sCMOS).

1038 ***In situ* hybridization.** Single molecule fluorescent *in situ* hybridization (RNAscope
1039 Multiplex Fluorescent Detection Kit v2, Advanced Cell Diagnostics) was used following
1040 the manufacturer protocol for fixed-frozen brains sample. Brain samples were sectioned
1041 at a thickness of 20 µm in a cryostat (CM1860, Leica). Sections were collected onto
1042 superfrost plus slides (Fisher Scientific) and transferred to a -80°C freezer. To prepare
1043 for the assay, brain sections were serially dehydrated with EtOH (50%, 75%, and 100%,
1044 each for 5 min) and then incubated in hydrogen peroxide for 10 min. Target retrieval
1045 was performed with RNAscope target retrieval reagents at 99°C for 5 min. The sections
1046 were then pretreated with Protease III (RNAscope) for 40 min at 40°C. RNAscope
1047 probes (Advanced Cell Diagnostics) for mCherry (Cat No. 431201-C3) and vGAT (Cat
1048 No. 424541) were hybridized at 40°C for 2h, serially amplified, and revealed with
1049 horseradish peroxidase, Opal Dye/TSA Plus fluorophore (Akoya Biosciences), and
1050 horseradish peroxidase blocker. Sections were cover-slipped with anti-fading mounting
1051 medium with DAPI (Vectashield, Vectorlabs) and kept in the refrigerator. Images were
1052 generated by using an epifluorescent microscope (Nikon, Eclipse NiE Fully Motorized

1053 Upright Microscope) equipped with a fluorescent lamp (X-Cite, 120 LED) and a digital
1054 camera (Andor Zyla 4.2 PLUS sCMOS). Expression of mCherry mRNA (red, Opal 620)
1055 and GAD67 mRNA (green, Opal 520) was determined by using an automated
1056 fluorescent threshold detector (NIS-Elements). Colabeled cells were manually counted
1057 by an experimenter by measuring either the percentage of mCherry positive neurons in
1058 PL that were also labeled with GAD67, or the percentage of GAD67 positive neurons in
1059 PL that were also labeled with mCherry.

1060 **Data analyses.** *Behavioral quantification and statistical analysis.* Rats were recorded
1061 with digital video cameras (Logitech C920) and behavioral responses were measured
1062 by using an automated video-tracking system (ANY-maze) or machine learning
1063 (DeepLabCut). Presses per minute were calculated by measuring the number of
1064 presses during the 30 s cue multiplied by two. All graphics and numerical values
1065 reported in the figures are presented as mean \pm s.e.m. Given that the different phases
1066 of the test have different duration, we have normalized the data in percentage to be able
1067 to compare the behavior of the animals across the different phases of the test. Shapiro
1068 Wilk normality test was performed before all the statistical analyses to determine
1069 parametrical or non-parametrical statistical tests, and reported in the Results section
1070 when the values showed non-normal distribution. For normal data, statistical
1071 significance was determined with paired or unpaired Student's t test, repeated-
1072 measures ANOVA followed by Bonferroni post-hoc comparisons (Prism 7), and Z-test or
1073 Fisher Exact Test, as indicated in the Results section, figure legends, and Table 1S. For
1074 non-parametric data, Wilcoxon test (paired groups) or Mann-Whitney test (unpaired
1075 groups) were performed. Effects sizes for pairwise comparisons or ANOVA were

1076 calculated by using Cohen's d or partial eta squared, respectively (Cohen, 1988;
1077 Richardson, 2011). Effect sizes < 0.2 were considered small, effects sizes between 0.2
1078 and 0.8 were considered medium, and effect sizes > 0.8 were considered large (Cohen,
1079 1988). Sample size (n) was based on estimations by power analysis with a level of
1080 significance of 0.05 and an expected effect size of 0.8.

1081 Single-unit analyses. Single-units were selected based on three principal components
1082 and waveform features such as valley-to-peak and amplitude measurements. The
1083 principal-component scores for unsorted waveforms were computed and plotted in a
1084 three (or two) dimensional principal-component space. Clusters containing similar valid
1085 waveforms were manually defined. After manually clustering similar valid waveforms, a
1086 group of spikes were considered from a single neuron if the waveforms formed a
1087 discrete, isolated, cluster in the principal-component space. A Commercial software
1088 (NeuroExplorer, NEXT Technologies) combined with Matlab (MathWorks) scripts, and
1089 Python scripting were implemented to calculate the spontaneous firing rate, changes in
1090 neural activity in response to food cues, lever presses, food dish entries, as well as the
1091 neural correlates of freezing, avoidance, and risk-assessment behaviors. The
1092 spontaneous firing rate was calculated by comparing the frequency of spike trains
1093 during the last 30 s of the food-seeking phase, odor phase, or conflict phase against the
1094 30 s prior to the beginning of each session. Food cue, lever press, and food dish
1095 responses were calculated by implementing Matlab scripts as Z-scores normalized to
1096 20 pre-cue bins of 300 ms. Neurons showing a Z-score > 2.58 ($p < 0.01$) during the first
1097 two-bins following the onset of the aligned event were classified as excitatory
1098 responses, whereas neurons showing a Z-score < -1.96 ($p < 0.05$) during the same first

1099 two-bins were classified as inhibitory responses. A temporal frequency separation was
1100 used to classify the food cue responses according to the pattern of activity, similar to a
1101 previous study ([Bezudnaya et al., 2006](#)). Neurons showing a transient increase in firing
1102 rate (< 600 ms duration) were classified as transient activity, whereas neurons showing
1103 a sustained increase in firing rate (≥ 900 ms duration) were classified as sustained
1104 activity (Z-score > 2.58 during the first 3 seconds after food cue onset).

1105 To analyze freezing, avoidance, and risk-assessment responses, the time onsets
1106 for each behavior were filtered by selecting only the events that lasted more than 1
1107 second and were not preceded by the same behavior during the previous 6 s (baseline).
1108 The final list of time onsets was entered into the single-unit recording files to create the
1109 events and temporally align them with the neuronal recordings. To increase the number
1110 of events during our analyses, we combined the behavioral responses emitted during
1111 the odor and conflict phases. Only animals exhibiting at least 6 events for each behavior
1112 were included. We used an interval criterium of 600 ms to select the neurons that
1113 responded close in time to the onset of the analyzed behavior (before or after), thereby
1114 avoiding potential neural activity contamination caused by other types of behavioral
1115 responses

1116 Data availability

1117 All the data that support the findings presented in this study are available from the
1118 corresponding author on reasonable request.

1119

1120

1121 **REFERENCES**

1122

- 1123 Ainslie G (1975) Specious reward: a behavioral theory of impulsiveness and impulse
1124 control. *Psychol Bull* 82:463-496.
- 1125 Allsop SA et al. (2018) Corticoamygdala Transfer of Socially Derived Information Gates
1126 Observational Learning. *Cell* 173:1329-1342 e1318.
- 1127 Amir A, Lee SC, Headley DB, Herzallah MM, Pare D (2015) Amygdala Signaling during
1128 Foraging in a Hazardous Environment. *J Neurosci* 35:12994-13005.
- 1129 Aupperle RL, Paulus MP (2010) Neural systems underlying approach and avoidance in
1130 anxiety disorders. *Dialogues Clin Neurosci* 12:517-531.
- 1131 Baeg EH, Kim YB, Jang J, Kim HT, Mook-Jung I, Jung MW (2001) Fast spiking and
1132 regular spiking neural correlates of fear conditioning in the medial prefrontal
1133 cortex of the rat. *Cereb Cortex* 11:441-451.
- 1134 Bari A, Theobald DE, Caprioli D, Mar AC, Aidoo-Micah A, Dalley JW, Robbins TW
1135 (2010) Serotonin modulates sensitivity to reward and negative feedback in a
1136 probabilistic reversal learning task in rats. *Neuropsychopharmacology* 35:1290-
1137 1301.
- 1138 Barker TV, Buzzell GA, Fox NA (2019) Approach, avoidance, and the detection of
1139 conflict in the development of behavioral inhibition. *New Ideas Psychol* 53:2-12.
- 1140 Berglind WJ, See RE, Fuchs RA, Ghee SM, Whitfield TW, Jr., Miller SW, McGinty JF
1141 (2007) A BDNF infusion into the medial prefrontal cortex suppresses cocaine
1142 seeking in rats. *Eur J Neurosci* 26:757-766.
- 1143 Beyeler A, Namburi P, Globler GF, Simonnet C, Calhoon GG, Conyers GF, Luck R,
1144 Wildes CP, Tye KM (2016) Divergent Routing of Positive and Negative
1145 Information from the Amygdala during Memory Retrieval. *Neuron* 90:348-361.
- 1146 Bezdudnaya T, Cano M, Bereshpolova Y, Stoelzel CR, Alonso JM, Swadlow HA (2006)
1147 Thalamic burst mode and inattention in the awake LGNd. *Neuron* 49:421-432.
- 1148 Blanchard DC, Griebel G, Pobbe R, Blanchard RJ (2011) Risk assessment as an
1149 evolved threat detection and analysis process. *Neurosci Biobehav Rev* 35:991-
1150 998.
- 1151 Bravo-Rivera H, Rubio Arzola P, Caban-Murillo A, Velez-Aviles AN, Ayala-Rosario SN,
1152 Quirk GJ (2021) Characterizing Different Strategies for Resolving Approach-
1153 Avoidance Conflict. *Front Neurosci* 15:608922.
- 1154 Breton JM, Charbit AR, Snyder BJ, Fong PTK, Dias EV, Himmels P, Lock H, Margolis
1155 EB (2019) Relative contributions and mapping of ventral tegmental area
1156 dopamine and GABA neurons by projection target in the rat. *J Comp Neurol*
1157 527:916-941.
- 1158 Burgos-Robles A, Vidal-Gonzalez I, Quirk GJ (2009) Sustained conditioned responses
1159 in prelimbic prefrontal neurons are correlated with fear expression and extinction
1160 failure. *J Neurosci* 29:8474-8482.
- 1161 Burgos-Robles A, Bravo-Rivera H, Quirk GJ (2013) Prelimbic and infralimbic neurons
1162 signal distinct aspects of appetitive instrumental behavior. *PLoS One* 8:e57575.
- 1163 Burgos-Robles A, Kimchi EY, Izadmehr EM, Porzenheim MJ, Ramos-Guasp WA, Nieh
1164 EH, Felix-Ortiz AC, Namburi P, Leppla CA, Presbrey KN, Anandalingam KK,
1165 Pagan-Rivera PA, Anahtar M, Beyeler A, Tye KM (2017) Amygdala inputs to

- 1166 prefrontal cortex guide behavior amid conflicting cues of reward and punishment.
1167 Nat Neurosci.
- 1168 Cain CK (2019) Avoidance Problems Reconsidered. *Curr Opin Behav Sci* 26:9-17.
- 1169 Capuzzo G, Floresco SB (2020) Prelimbic and Infralimbic Prefrontal Regulation of
1170 Active and Inhibitory Avoidance and Reward-Seeking. *J Neurosci* 40:4773-4787.
- 1171 Chen BT, Yau HJ, Hatch C, Kusumoto-Yoshida I, Cho SL, Hopf FW, Bonci A (2013)
1172 Rescuing cocaine-induced prefrontal cortex hypoactivity prevents compulsive
1173 cocaine seeking. *Nature* 496:359-362.
- 1174 Choi EA, McNally GP (2017) Paraventricular Thalamus Balances Danger and Reward.
1175 *J Neurosci* 37:3018-3029.
- 1176 Choi EA, Jean-Richard-Dit-Bressel P, Clifford CWG, McNally GP (2019) Paraventricular
1177 Thalamus Controls Behavior during Motivational Conflict. *J Neurosci* 39:4945-
1178 4958.
- 1179 Churchland AK, Kiani R, Chaudhuri R, Wang XJ, Pouget A, Shadlen MN (2011)
1180 Variance as a signature of neural computations during decision making. *Neuron*
1181 69:818-831.
- 1182 Cohen J (1988) *Statistical Power Analysis for the Behavioral Sciences* (2nd edition).
1183 Hillsdale: Erlbaum Associates.
- 1184 Cohen JY, Haesler S, Vong L, Lowell BB, Uchida N (2012) Neuron-type-specific signals
1185 for reward and punishment in the ventral tegmental area. *Nature* 482:85-88.
- 1186 Courtin J, Chaudun F, Rozeske RR, Karalis N, Gonzalez-Campo C, Wurtz H, Abdi A,
1187 Baufreton J, Bienvenu TC, Herry C (2014) Prefrontal parvalbumin interneurons
1188 shape neuronal activity to drive fear expression. *Nature* 505:92-96.
- 1189 Cummings KA, Clem RL (2020) Prefrontal somatostatin interneurons encode fear
1190 memory. *Nat Neurosci* 23:61-74.
- 1191 Dejean C, Courtin J, Karalis N, Chaudun F, Wurtz H, Bienvenu TC, Herry C (2016)
1192 Prefrontal neuronal assemblies temporally control fear behaviour. *Nature*
1193 535:420-424.
- 1194 Dellu-Hagedorn F, Rivalan M, Fitoussi A, De Deurwaerdere P (2018) Inter-individual
1195 differences in the impulsive/compulsive dimension: deciphering related
1196 dopaminergic and serotonergic metabolisms at rest. *Philos Trans R Soc Lond B*
1197 *Biol Sci* 373.
- 1198 Diehl MM, Bravo-Rivera C, Rodriguez-Romaguera J, Pagan-Rivera PA, Burgos-Robles
1199 A, Roman-Ortiz C, Quirk GJ (2018) Active avoidance requires inhibitory signaling
1200 in the rodent prelimbic prefrontal cortex. *Elife* 7.
- 1201 Dimidschstein J et al. (2016) A viral strategy for targeting and manipulating interneurons
1202 across vertebrate species. *Nat Neurosci* 19:1743-1749.
- 1203 Do-Monte FH, Quinones-Laracuente K, Quirk GJ (2015) A temporal shift in the circuits
1204 mediating retrieval of fear memory. *Nature* 519:460-463.
- 1205 Do-Monte FH, Rodriguez-Romaguera J, Rosas-Vidal LE, Quirk GJ (2013) Deep brain
1206 stimulation of the ventral striatum increases BDNF in the fear extinction circuit.
1207 *Front Behav Neurosci* 7:102.
- 1208 Do Monte FH, Quirk GJ, Li B, Penzo MA (2016) Retrieving fear memories, as time goes
1209 by. *Mol Psychiatry* 21:1027-1036.

- 1210 Emmons EB, Ruggiero RN, Kelley RM, Parker KL, Narayanan NS (2016) Corticostriatal
1211 Field Potentials Are Modulated at Delta and Theta Frequencies during Interval-
1212 Timing Task in Rodents. *Front Psychol* 7:459.
- 1213 Engelke DS, Zhang XO, O'Malley JJ, Fernandez-Leon JA, Li S, Kirouac GJ, Beierlein
1214 M, Do-Monte FH (2021) A hypothalamic-thalamostriatal circuit that controls
1215 approach-avoidance conflict in rats. *Nat Commun* 12:2517.
- 1216 Ferenczi EA, Zalocusky KA, Liston C, Grosenick L, Warden MR, Amatya D, Katovich K,
1217 Mehta H, Patenaude B, Ramakrishnan C, Kalanithi P, Etkin A, Knutson B, Glover
1218 GH, Deisseroth K (2016) Prefrontal cortical regulation of brainwide circuit
1219 dynamics and reward-related behavior. *Science* 351:aac9698.
- 1220 Flagel SB, Watson SJ, Robinson TE, Akil H (2007) Individual differences in the
1221 propensity to approach signals vs goals promote different adaptations in the
1222 dopamine system of rats. *Psychopharmacology (Berl)* 191:599-607.
- 1223 Flagel SB, Clark JJ, Robinson TE, Mayo L, Czuj A, Willuhn I, Akers CA, Clinton SM,
1224 Phillips PE, Akil H (2011) A selective role for dopamine in stimulus-reward
1225 learning. *Nature* 469:53-57.
- 1226 Gabbott PL, Warner TA, Jays PR, Salway P, Busby SJ (2005) Prefrontal cortex in the
1227 rat: projections to subcortical autonomic, motor, and limbic centers. *J Comp*
1228 *Neurol* 492:145-177.
- 1229 Gaykema RP, Nguyen XM, Boehret JM, Lambeth PS, Joy-Gaba J, Warthen DM, Scott
1230 MM (2014) Characterization of excitatory and inhibitory neuron activation in the
1231 mouse medial prefrontal cortex following palatable food ingestion and food driven
1232 exploratory behavior. *Front Neuroanat* 8:60.
- 1233 Geller I (1960) The acquisition and extinction of conditioned suppression as a function
1234 of the base-line reinforcer. *J Exp Anal Behav* 3:235-240.
- 1235 Gradinaru V, Mogri M, Thompson KR, Henderson JM, Deisseroth K (2009) Optical
1236 deconstruction of parkinsonian neural circuitry. *Science* 324:354-359.
- 1237 Grant RI, Doncheck EM, Vollmer KM, Winston KT, Romanova EV, Siegler PN, Holman
1238 H, Bowen CW, Otis JM (2021) Specialized coding patterns among dorsomedial
1239 prefrontal neuronal ensembles predict conditioned reward seeking. *Elife* 10.
- 1240 Haight JL, Fuller ZL, Fraser KM, Flagel SB (2017) A food-predictive cue attributed with
1241 incentive salience engages subcortical afferents and efferents of the
1242 paraventricular nucleus of the thalamus. *Neuroscience* 340:135-152.
- 1243 Harris AZ, Gordon JA (2015) Long-range neural synchrony in behavior. *Annu Rev*
1244 *Neurosci* 38:171-194.
- 1245 Horst NK, Laubach M (2013) Reward-related activity in the medial prefrontal cortex is
1246 driven by consumption. *Front Neurosci* 7:56.
- 1247 Hu H (2016) Reward and Aversion. *Annu Rev Neurosci* 39:297-324.
- 1248 Hyman JM, Hasselmo ME, Seamans JK (2011) What is the Functional Relevance of
1249 Prefrontal Cortex Entrainment to Hippocampal Theta Rhythms? *Front Neurosci*
1250 5:24.
- 1251 Jean-Richard-Dit-Bressel P, Ma C, Bradfield LA, Killcross S, McNally GP (2019)
1252 Punishment insensitivity emerges from impaired contingency detection, not
1253 aversion insensitivity or reward dominance. *Elife* 8.
- 1254 Jensen J, Walter H (2014) Incentive motivational salience and the human brain. *Restor*
1255 *Neurol Neurosci* 32:141-147.

- 1256 Karalis N, Dejean C, Chaudun F, Khoder S, Rozeske RR, Wurtz H, Bagur S,
1257 Benchenane K, Sirota A, Courtin J, Herry C (2016) 4-Hz oscillations synchronize
1258 prefrontal-amygdala circuits during fear behavior. *Nat Neurosci*.
- 1259 Kim CK, Ye L, Jennings JH, Pichamoorthy N, Tang DD, Yoo AW, Ramakrishnan C,
1260 Deisseroth K (2017) Molecular and Circuit-Dynamical Identification of Top-Down
1261 Neural Mechanisms for Restraint of Reward Seeking. *Cell* 170:1013-1027 e1014.
- 1262 Kim EJ, Kim N, Kim HT, Choi JS (2013) The prelimbic cortex is critical for context-
1263 dependent fear expression. *Front Behav Neurosci* 7:73.
- 1264 Kim EJ, Kong MS, Park SG, Mizumori SJY, Cho J, Kim JJ (2018) Dynamic coding of
1265 predatory information between the prelimbic cortex and lateral amygdala in
1266 foraging rats. *Sci Adv* 4:eaar7328.
- 1267 Kirlic N, Young J, Aupperle RL (2017) Animal to human translational paradigms relevant
1268 for approach avoidance conflict decision making. *Behav Res Ther* 96:14-29.
- 1269 Kroener S, Chandler LJ, Phillips PE, Seamans JK (2009) Dopamine modulates
1270 persistent synaptic activity and enhances the signal-to-noise ratio in the
1271 prefrontal cortex. *PLoS One* 4:e6507.
- 1272 Kryptos AM, Eftting M, Kindt M, Beckers T (2015) Avoidance learning: a review of
1273 theoretical models and recent developments. *Front Behav Neurosci* 9:189.
- 1274 Kyriazi P, Headley DB, Pare D (2020) Different Multidimensional Representations
1275 across the Amygdalo-Prefrontal Network during an Approach-Avoidance Task.
1276 *Neuron* 107:717-730 e715.
- 1277 Likhtik E, Paz R (2015) Amygdala-prefrontal interactions in (mal)adaptive learning.
1278 *Trends Neurosci* 38:158-166.
- 1279 Likhtik E, Stujenske JM, Topiwala MA, Harris AZ, Gordon JA (2014) Prefrontal
1280 entrainment of amygdala activity signals safety in learned fear and innate
1281 anxiety. *Nat Neurosci* 17:106-113.
- 1282 Lima SQ, Hromadka T, Znamenskiy P, Zador AM (2009) PINP: a new method of
1283 tagging neuronal populations for identification during in vivo electrophysiological
1284 recording. *PLoS One* 4:e6099.
- 1285 Marquis JP, Killcross S, Haddon JE (2007) Inactivation of the prelimbic, but not
1286 infralimbic, prefrontal cortex impairs the contextual control of response conflict in
1287 rats. *Eur J Neurosci* 25:559-566.
- 1288 Mathis A, Mamidanna P, Cury KM, Abe T, Murthy VN, Mathis MW, Bethge M (2018)
1289 DeepLabCut: markerless pose estimation of user-defined body parts with deep
1290 learning. *Nat Neurosci* 21:1281-1289.
- 1291 McDonald AJ (1991) Organization of amygdaloid projections to the prefrontal cortex and
1292 associated striatum in the rat. *Neuroscience* 44:1-14.
- 1293 McGinley MJ, David SV, McCormick DA (2015) Cortical Membrane Potential Signature
1294 of Optimal States for Sensory Signal Detection. *Neuron* 87:179-192.
- 1295 McGinty JF, Otis JM (2020) Heterogeneity in the Paraventricular Thalamus: The Traffic
1296 Light of Motivated Behaviors. *Front Behav Neurosci* 14:590528.
- 1297 McNaughton N, Corr PJ (2014) Approach, avoidance, and their conflict: the problem of
1298 anchoring. *Front Syst Neurosci* 8:124.
- 1299 Millan EZ, Ong Z, McNally GP (2017) Paraventricular thalamus: Gateway to feeding,
1300 appetitive motivation, and drug addiction. *Prog Brain Res* 235:113-137.

- 1301 Moorman DE, Aston-Jones G (2015) Prefrontal neurons encode context-based
1302 response execution and inhibition in reward seeking and extinction. *Proc Natl*
1303 *Acad Sci U S A* 112:9472-9477.
- 1304 Morales I, Berridge KC (2020) 'Liking' and 'wanting' in eating and food reward: Brain
1305 mechanisms and clinical implications. *Physiol Behav* 227:113152.
- 1306 Nair-Roberts RG, Chatelain-Badie SD, Benson E, White-Cooper H, Bolam JP, Ungless
1307 MA (2008) Stereological estimates of dopaminergic, GABAergic and
1308 glutamatergic neurons in the ventral tegmental area, substantia nigra and
1309 retrorubral field in the rat. *Neuroscience* 152:1024-1031.
- 1310 Namburi P, Beyeler A, Yorozu S, Calhoun GG, Halbert SA, Wichmann R, Holden SS,
1311 Mertens KL, Anahtar M, Felix-Ortiz AC, Wickersham IR, Gray JM, Tye KM (2015)
1312 A circuit mechanism for differentiating positive and negative associations. *Nature*
1313 520:675-678.
- 1314 Narayanan NS, Cavanagh JF, Frank MJ, Laubach M (2013) Common medial frontal
1315 mechanisms of adaptive control in humans and rodents. *Nat Neurosci* 16:1888-
1316 1895.
- 1317 Oberrauch S, Sigrist H, Sautter E, Gerster S, Bach DR, Pryce CR (2019) Establishing
1318 operant conflict tests for the translational study of anxiety in mice.
1319 *Psychopharmacology (Berl)* 236:2527-2541.
- 1320 Orsini CA, Heshmati SC, Garman TS, Wall SC, Bizon JL, Setlow B (2018) Contributions
1321 of medial prefrontal cortex to decision making involving risk of punishment.
1322 *Neuropharmacology* 139:205-216.
- 1323 Otis JM, Namboodiri VM, Matan AM, Voets ES, Mohorn EP, Kosyk O, McHenry JA,
1324 Robinson JE, Resendez SL, Rossi MA, Stuber GD (2017) Prefrontal cortex
1325 output circuits guide reward seeking through divergent cue encoding. *Nature*
1326 543:103-107.
- 1327 Padilla-Coreano N, Canetta S, Mikofsky RM, Alway E, Passecker J, Myroshnychenko
1328 MV, Garcia-Garcia AL, Warren R, Teboul E, Blackman DR, Morton MP, Hupalo
1329 S, Tye KM, Kellendonk C, Kupferschmidt DA, Gordon JA (2019) Hippocampal-
1330 Prefrontal Theta Transmission Regulates Avoidance Behavior. *Neuron* 104:601-
1331 610 e604.
- 1332 Park J, Moghaddam B (2017) Risk of punishment influences discrete and coordinated
1333 encoding of reward-guided actions by prefrontal cortex and VTA neurons. *Elife* 6.
- 1334 Penzo MA, Gao C (2021) The paraventricular nucleus of the thalamus: an integrative
1335 node underlying homeostatic behavior. *Trends Neurosci*.
- 1336 Pi HJ, Hangya B, Kvitsiani D, Sanders JI, Huang ZJ, Kepecs A (2013) Cortical
1337 interneurons that specialize in disinhibitory control. *Nature* 503:521-524.
- 1338 Piantadosi PT, Yeates DCM, Floresco SB (2020) Prefrontal cortical and nucleus
1339 accumbens contributions to discriminative conditioned suppression of reward-
1340 seeking. *Learn Mem* 27:429-440.
- 1341 Popa D, Duvarci S, Popescu AT, Lena C, Pare D (2010) Coherent amygdalocortical
1342 theta promotes fear memory consolidation during paradoxical sleep. *Proc Natl*
1343 *Acad Sci U S A* 107:6516-6519.
- 1344 Punter PH (1983) Measurement of human olfactory thresholds for several groups of
1345 structurally related compounds. *Chem Senses* 7:215-235.

- 1346 Radke AK, Nakazawa K, Holmes A (2015) Cortical GluN2B deletion attenuates
1347 punished suppression of food reward-seeking. *Psychopharmacology (Berl)*
1348 232:3753-3761.
- 1349 Richardson JTE (2011) Eta squared and partial eta squared as measures of effect size
1350 in educational research. *Educational Research Review* 6:135-147.
- 1351 Robinson TE, Flagel SB (2009) Dissociating the predictive and incentive motivational
1352 properties of reward-related cues through the study of individual differences. *Biol*
1353 *Psychiatry* 65:869-873.
- 1354 Robinson TE, Yager LM, Cogan ES, Saunders BT (2014) On the motivational properties
1355 of reward cues: Individual differences. *Neuropharmacology* 76 Pt B:450-459.
- 1356 Sangha S, Robinson PD, Greba Q, Davies DA, Howland JG (2014) Alterations in
1357 reward, fear and safety cue discrimination after inactivation of the rat prelimbic
1358 and infralimbic cortices. *Neuropsychopharmacology* 39:2405-2413.
- 1359 Santana N, Bortolozzi A, Serrats J, Mengod G, Artigas F (2004) Expression of
1360 serotonin1A and serotonin2A receptors in pyramidal and GABAergic neurons of
1361 the rat prefrontal cortex. *Cereb Cortex* 14:1100-1109.
- 1362 Schultz W (2015) Neuronal Reward and Decision Signals: From Theories to Data.
1363 *Physiol Rev* 95:853-951.
- 1364 Serrano-Barroso A, Vargas JP, Diaz E, O'Donnell P, Lopez JC (2019) Sign and goal
1365 tracker rats process differently the incentive salience of a conditioned stimulus.
1366 *PLoS One* 14:e0223109.
- 1367 Sharpe MJ, Killcross S (2015) The prelimbic cortex directs attention toward predictive
1368 cues during fear learning. *Learn Mem* 22:289-293.
- 1369 Sierra-Mercado D, Padilla-Coreano N, Quirk GJ (2011) Dissociable roles of prelimbic
1370 and infralimbic cortices, ventral hippocampus, and basolateral amygdala in the
1371 expression and extinction of conditioned fear. *Neuropsychopharmacology*
1372 36:529-538.
- 1373 Simon NW, Gilbert RJ, Mayse JD, Bizon JL, Setlow B (2009) Balancing risk and reward:
1374 a rat model of risky decision making. *Neuropsychopharmacology* 34:2208-2217.
- 1375 Smith KS, Berridge KC, Aldridge JW (2011) Disentangling pleasure from incentive
1376 salience and learning signals in brain reward circuitry. *Proc Natl Acad Sci U S A*
1377 108:E255-264.
- 1378 Sotres-Bayon F, Sierra-Mercado D, Pardilla-Delgado E, Quirk GJ (2012) Gating of fear
1379 in prelimbic cortex by hippocampal and amygdala inputs. *Neuron* 76:804-812.
- 1380 St Onge JR, Floresco SB (2009) Dopaminergic modulation of risk-based decision
1381 making. *Neuropsychopharmacology* 34:681-697.
- 1382 Stujenske JM, Likhtik E, Topiwala MA, Gordon JA (2014) Fear and safety engage
1383 competing patterns of theta-gamma coupling in the basolateral amygdala.
1384 *Neuron* 83:919-933.
- 1385 Sun X, Bernstein MJ, Meng M, Rao S, Sorensen AT, Yao L, Zhang X, Anikeeva PO, Lin
1386 Y (2020) Functionally Distinct Neuronal Ensembles within the Memory Engram.
1387 *Cell* 181:410-423 e417.
- 1388 Tan KR, Yvon C, Turiault M, Mirzabekov JJ, Doehner J, Labouebe G, Deisseroth K, Tye
1389 KM, Luscher C (2012) GABA neurons of the VTA drive conditioned place
1390 aversion. *Neuron* 73:1173-1183.

- 1391 Tomie A, Aguado AS, Pohorecky LA, Benjamin D (2000) Individual differences in
1392 pavlovian autoshaping of lever pressing in rats predict stress-induced
1393 corticosterone release and mesolimbic levels of monoamines. *Pharmacol*
1394 *Biochem Behav* 65:509-517.
- 1395 Totah NK, Jackson ME, Moghaddam B (2013) Preparatory attention relies on dynamic
1396 interactions between prelimbic cortex and anterior cingulate cortex. *Cereb Cortex*
1397 23:729-738.
- 1398 Treanor M, Barry TJ (2017) Treatment of avoidance behavior as an adjunct to exposure
1399 therapy: Insights from modern learning theory. *Behav Res Ther* 96:30-36.
- 1400 Tye KM, Prakash R, Kim SY, Fenno LE, Grosenick L, Zarabi H, Thompson KR,
1401 Gradinaru V, Ramakrishnan C, Deisseroth K (2011) Amygdala circuitry mediating
1402 reversible and bidirectional control of anxiety. *Nature* 471:358-362.
- 1403 van Zessen R, Phillips JL, Budygin EA, Stuber GD (2012) Activation of VTA GABA
1404 neurons disrupts reward consumption. *Neuron* 73:1184-1194.
- 1405 Verharen JPH, van den Heuvel MW, Luijendijk M, Vanderschuren L, Adan RAH (2019)
1406 Corticolimbic Mechanisms of Behavioral Inhibition under Threat of Punishment. *J*
1407 *Neurosci* 39:4353-4364.
- 1408 Vertes RP (2004) Differential projections of the infralimbic and prelimbic cortex in the
1409 rat. *Synapse* 51:32-58.
- 1410 Vidal-Gonzalez I, Vidal-Gonzalez B, Rauch SL, Quirk GJ (2006) Microstimulation
1411 reveals opposing influences of prelimbic and infralimbic cortex on the expression
1412 of conditioned fear. *Learn Mem* 13:728-733.
- 1413 Vogel JR, Beer B, Clody DE (1971) A simple and reliable conflict procedure for testing
1414 anti-anxiety agents. *Psychopharmacologia* 21:1-7.
- 1415 Volkow ND, Wang GJ, Fowler JS, Tomasi D, Baler R (2012) Food and drug reward:
1416 overlapping circuits in human obesity and addiction. *Curr Top Behav Neurosci*
1417 11:1-24.
- 1418 Wakabayashi KT, Feja M, Baidur AN, Bruno MJ, Bhimani RV, Park J, Hausknecht K,
1419 Shen RY, Haj-Dahmane S, Bass CE (2019) Chemogenetic activation of ventral
1420 tegmental area GABA neurons, but not mesoaccumbal GABA terminals, disrupts
1421 responding to reward-predictive cues. *Neuropsychopharmacology* 44:372-380.
- 1422 Warthen DM, Lambeth PS, Ottolini M, Shi Y, Barker BS, Gaykema RP, Newmyer BA,
1423 Joy-Gaba J, Ohmura Y, Perez-Reyes E, Guler AD, Patel MK, Scott MM (2016)
1424 Activation of Pyramidal Neurons in Mouse Medial Prefrontal Cortex Enhances
1425 Food-Seeking Behavior While Reducing Impulsivity in the Absence of an Effect
1426 on Food Intake. *Front Behav Neurosci* 10:63.
- 1427 Widge AS, Heilbronner SR, Hayden BY (2019) Prefrontal cortex and cognitive control:
1428 new insights from human electrophysiology. *F1000Res* 8.
- 1429 Zack GW, Rogers WE, Latt SA (1977) Automatic measurement of sister chromatid
1430 exchange frequency. *J Histochem Cytochem* 25:741-753.
- 1431 Zhang X, Kim J, Tonegawa S (2020) Amygdala Reward Neurons Form and Store Fear
1432 Extinction Memory. *Neuron* 105:1077-1093 e1077.

1433

FIGURE 1

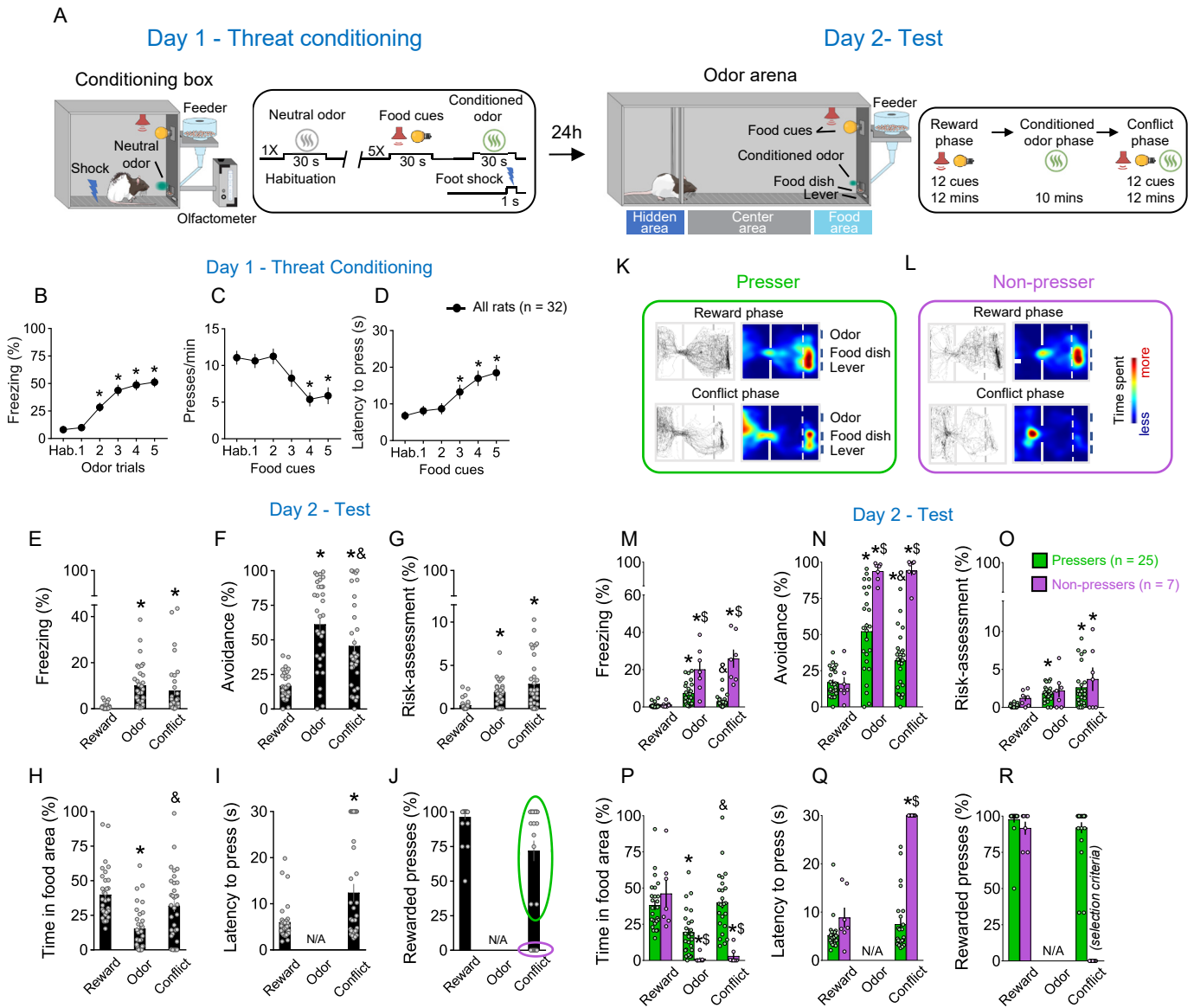


Figure 1. Rats show individual variability in reward-seeking responses during an approach-avoidance conflict test. (A) Schematic and timeline of the approach-avoidance conflict test. **(B-D)** Rats exhibited an increase in the percentage of time freezing (Shapiro-Wilk normality test, $p < 0.001$, Friedman Test, Friedman statistic = 84.08, $p < 0.001$, Dunn's *post-hoc*, $p < 0.001$) and a reduction in lever presses (Shapiro-Wilk normality test, $p < 0.001$, Friedman Test, Friedman statistic = 35.11, $p < 0.001$, Dunn's *post-hoc*, $p < 0.001$) with a higher latency to press the lever (Shapiro-Wilk normality test, $p < 0.001$, Friedman Test, Friedman statistic = 29.45, $p < 0.001$, Dunn's *post-hoc*, $p < 0.001$) during the olfactory threat conditioning session on day 1 ($n = 32$), when compared to before the shock. **(E-G)** Patterns of defensive responses and food seeking during the different phases (reward, odor, conflict) of the test session on day 2. Rats showed an increase in defensive responses characterized by an augment in the percentage of time exhibiting (E) freezing (Shapiro-Wilk normality test, $p < 0.05$, Friedman Test, Friedman statistic = 40.46, $p < 0.001$, Dunn's *post-hoc*, $p < 0.001$), (F) avoidance (Shapiro-Wilk normality test, $p < 0.05$, Friedman Test, Friedman statistic = 31.67, $p < 0.001$, Dunn's *post-hoc*, $p < 0.001$) and (G) risk-assessment (Shapiro-Wilk normality test, $p < 0.05$, Friedman Test, Friedman statistic = 29.86, $p < 0.001$, Dunn's *post-hoc*, $p < 0.001$); and a decrease in the (H) percentage of time spent in the food area (Shapiro-Wilk normality test, $p < 0.05$, Friedman Test, Friedman statistic = 32.19, $p < 0.001$, Dunn's *post-hoc*, $p < 0.001$) during the odor presentation, when compared to the reward phase. Rats' defensive responses were significantly attenuated during the conflict phase as evidenced by a reduction in the percentage of time (F) avoiding the odor ($p = 0.0031$) and an increase in the percentage of time (H) approaching the food area ($p < 0.001$), when compared to the odor phase. **(I-J)** Two different behavioral phenotypes emerged during the conflict phase: rats that continued to press the lever (*Pressers*, green circle, $n = 25$) and rats that showed a complete suppression in lever pressing (*Non-pressers*, purple circle, $n = 7$). Rewarded presses were calculated as the percentage of the 12 cue trials in which rats pressed the lever. **(K-L)** Representative tracks and heatmaps of time spent in each compartment of the arena for a (K) *Presser* or a (L) *Non-Pressers* rat during the test session. **(M-R)** Patterns of defensive responses and food seeking during the different phases (reward, odor, conflict) of the test session on day 2 after separating the animals into *Pressers* and *Non-pressers*. When compared to *Non-Pressers*, *Pressers* showed reduced defensive responses characterized by an attenuation in the percentage of time exhibiting (M) freezing ($F_{(2, 60)} = 29.54$, $p < 0.001$) and (N) avoidance responses ($F_{(2, 60)} = 23.27$, $p < 0.001$), and an augment in the percentage of time (P) approaching the food area ($F_{(2, 60)} = 22.49$, $p < 0.001$) during both the odor and the conflict phases (Bonferroni post-hoc test - odor phase, $p = 0.0453$; conflict phase, $p < 0.001$). (Q) *Non-Pressers* showed increased latency to press the lever during the conflict phase when compared to the reward phase or to *Pressers* in the same phase ($F_{(1, 30)} = 55.14$, $p < 0.001$, Bonferroni post-hoc test – all p 's < 0.001). (R) The percentage of rewarded trials was used as a binary criterium for group classification. Data shown as mean \pm SEM. One-way or two-way ANOVA repeated measures followed by Bonferroni *post-hoc* test, all * p 's < 0.05 compared to the same group during the reward phase, all & p 's < 0.05 compared to the same group during the odor phase, all \$ p 's < 0.05 compared to *Pressers* during the same phase. All statistical analysis details are presented in table S1. See also Supplementary Fig. 1 and Supplementary Video 1.

FIGURE 2

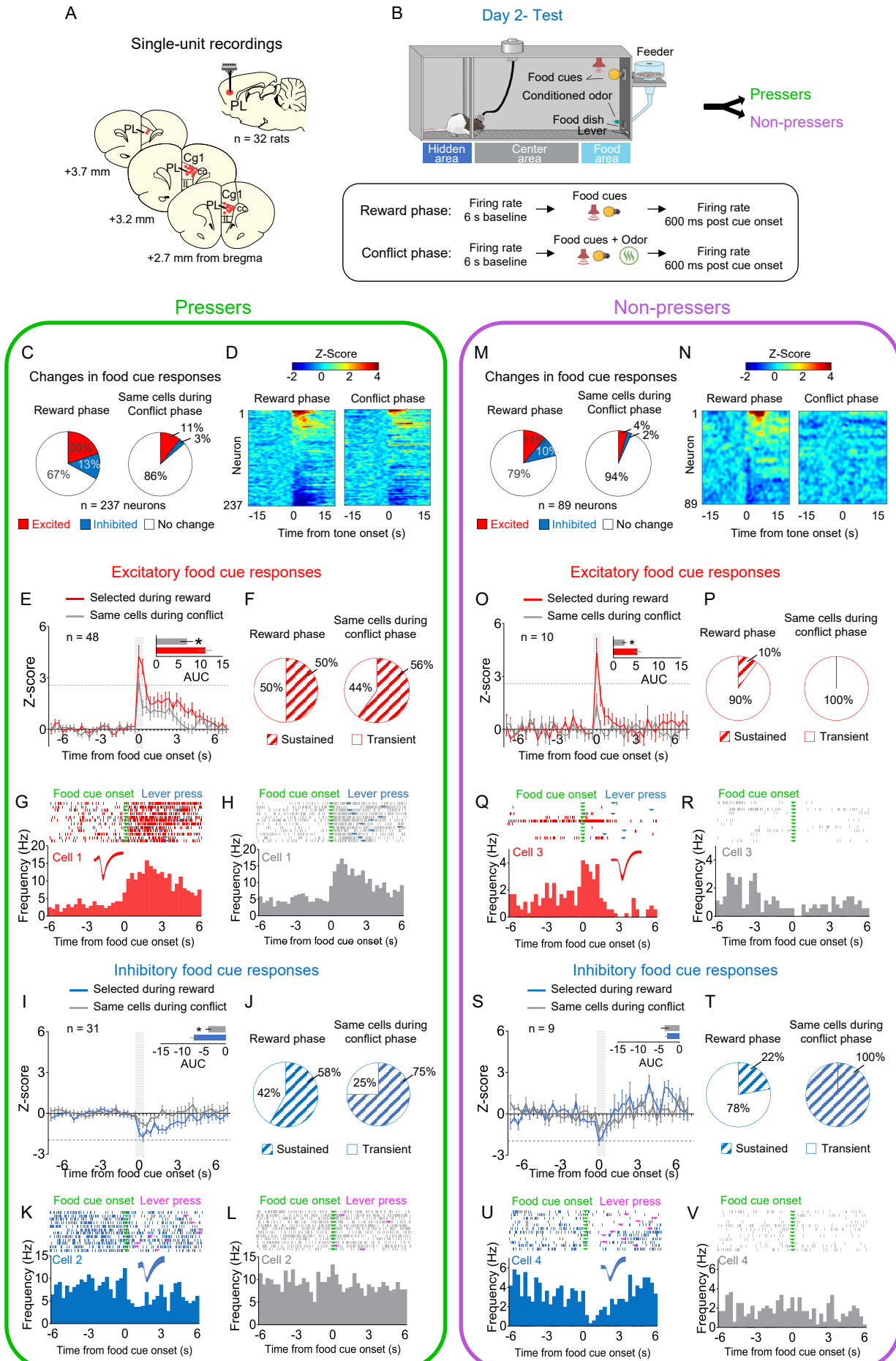


Figure 2. PL neurons respond differently to reward cues in Pressers vs. Non-Pressers during conflict (A) Diagram of the electrode placements in PL. (B) Schematic and timeline of PL recordings for food cue responses during of the approach-avoidance conflict test (12 food cues per phase). (C) Pie charts showing changes in PL firing rate in response to food cues during reward (left) vs. conflict (right) phases for *Pressers* (n = 237 neurons from 25 rats, Fisher Exact Test, responsive during reward phase: n = 79, responsive during conflict phase: n = 32, p < 0.001; excited during reward phase: n = 48, excited during conflict phase: n = 25, p = 0.0049; inhibited during reward phase: n = 31, inhibited during conflict phase: n = 7, p < 0.001). (D) Heatmap of Z-scored neural activities for PL neurons selected during reward phase and tracked to conflict phase. (E) Average peri-stimulus time histograms (PSTHs) for all PL neurons showing excitatory food cue responses (Z-score > 2.58, dotted line) during reward (red line) compared to the same cells during conflict (gray line). E, Inset: Differences in the positive area under the curve (AUC) between the two phases (Shapiro-Wilk normality test, p < 0.001; Wilcoxon test, W = -824, excitatory responses reward phase vs. conflict phase, p < 0.001). (F) Pie charts showing the percentage of sustained vs. transient excitatory food-cue responses in PL neurons during the reward phase with the same neurons tracked during the conflict phase. (G-H) Representative PSTHs for a PL neuron showing excitatory responses to food cues during the (G) reward phase vs. the same neuron during the (H) conflict phase. (I) Average PSTHs for all PL neurons showing inhibitory food cue responses (Z-score < -1.96, dotted line) during reward (blue line) compared to the same cells during conflict (gray line). I, Inset: Differences in the negative AUC between the two phases (Shapiro-Wilk normality test, p < 0.001; Wilcoxon test, W = 367, inhibitory responses reward phase vs. conflict phase, p < 0.001). (J) Pie charts showing the percentage of sustained vs. transient inhibitory food-cue responses in PL neurons during the reward phase with the same neurons tracked during the conflict phase. (K-L) Representative PSTHs for a PL neuron showing inhibitory responses to food cues during the reward phase (K) vs. the same neuron during the conflict phase (L). (M) Pie charts showing changes in PL firing rate in response to food cues during reward (left) vs. conflict (right) phases for *Non-Pressers* (n= 89 neurons from 7 rats; Fisher Exact Test, responsive during reward phase: n = 19, responsive during conflict phase: n = 6, p < 0.0086; excited during reward phase: n = 10, excited during conflict phase: n = 4, p = 0.162; inhibited during reward phase: n = 9, inhibited during conflict phase: n = 2, p = 0.057). (N-O) Same as D-E, but for *Non-Pressers*. O, Inset: Differences in the positive AUC between the two phases (Paired Student's t-test, t = 2.34, p = 0.043). (P-S) Same as F-I, but for *Non-Pressers*. S, Inset: Differences in the negative AUC between the two phases (Paired Student's t-test, t = 0.59, p = 0.569) (T-V) Same as J-L, but for *Non-Pressers*. The threshold used to identify significant differences per neurons was Z-score > 2.58 for excitation and Z-score < -1.96 for inhibition. Legend: cc, corpus callosum, CG1, anterior cingulate cortex; IL, infralimbic cortex. All statistical analysis details are presented in table S1. See also Supplementary Figs. 2-5.

FIGURE 3

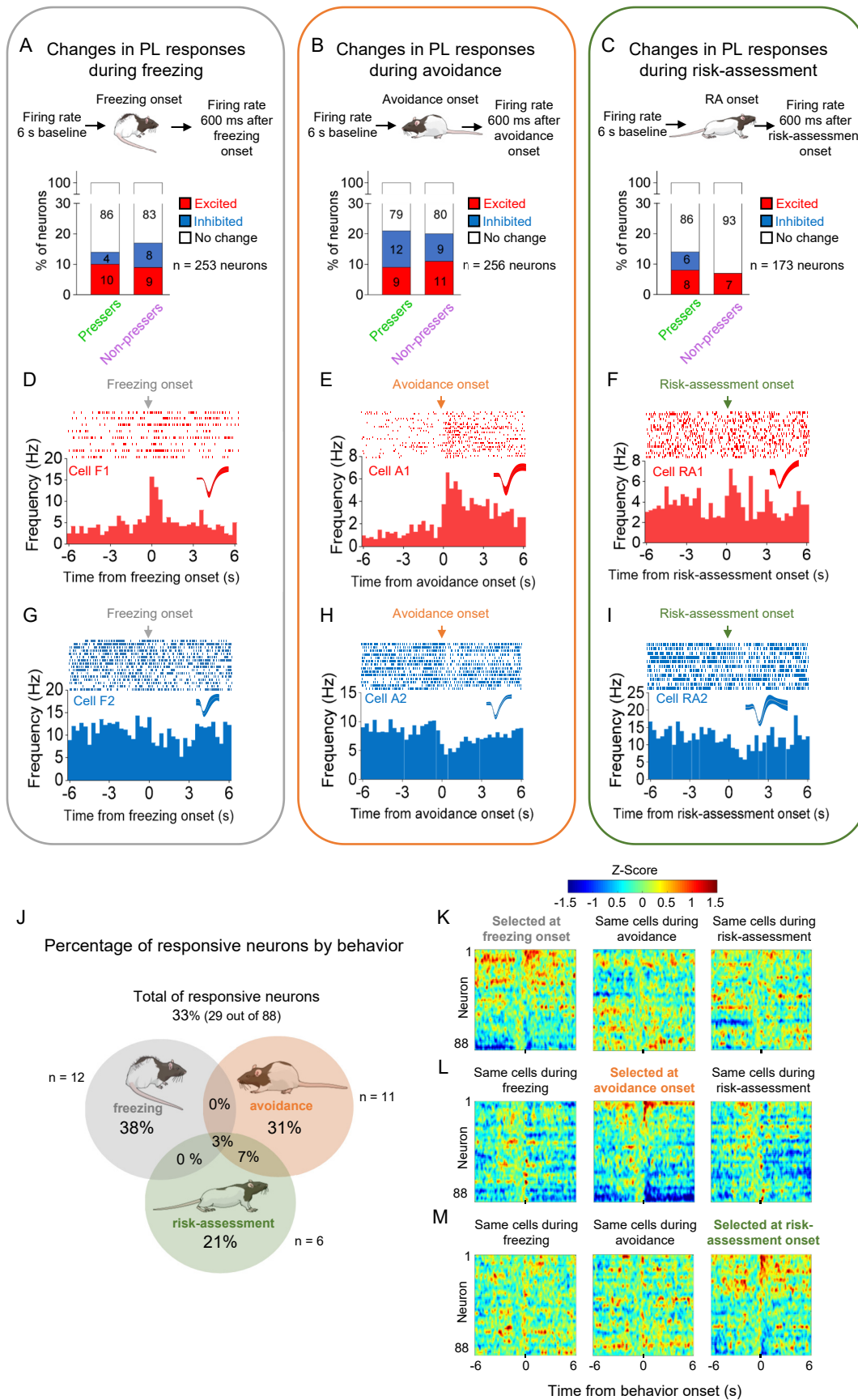


Figure 3. PL activity correlates with the onset of freezing, avoidance or risk-assessment behaviors in both *Pressers* and *Non-Pressers*. **(A-C)** Both *Pressers* and *Non-Pressers* showed the same number and proportion of excitatory and inhibitory PL responses during the onset of (A) freezing (Fisher Exact Test, responsive neurons in *Pressers*: 22 neurons, in *Non-Pressers*: 15 neurons, $p = 0.462$), (B) avoidance (Fisher Exact Test, responsive neurons in *Pressers*: 43 neurons, in *Non-Pressers*: 9 neurons, $p = 0.999$) or (C) risk-assessment (RA, Fisher Exact Test, responsive neurons in *Pressers*: 12 neurons, in *Non-Pressers*: 6 neurons, $p = 0.318$) behaviors. **(D-F)** Representative PSTHs for distinct PL neurons showing excitatory responses at the onset of (D) freezing, (E) avoidance or (F) risk-assessment behaviors. **(G-I)** Representative PSTHs for distinct PL neurons showing inhibitory responses at the onset of freezing (G), avoidance (H) or risk-assessment (I) behaviors. **(J)** Venn Diagram showing the percentage of all PL responsive neurons (29 out of 88 neurons) by behavior. Most of the responsive neurons responded selectively at the onset of one of the behaviors. **(K-M)** Heatmap of Z-scored neural activities for PL neurons selected at the onset of freezing (K), avoidance (L) or risk-assessment behavior (M) with the same cells tracked during the other behaviors. The threshold used to identify significant differences per neurons was Z-score > 2.58 for excitation and Z-score < -1.96 for inhibition. n.s. = non-significant. All statistical analysis details are presented in table S1. See also Supplementary Fig. 6.

FIGURE 4

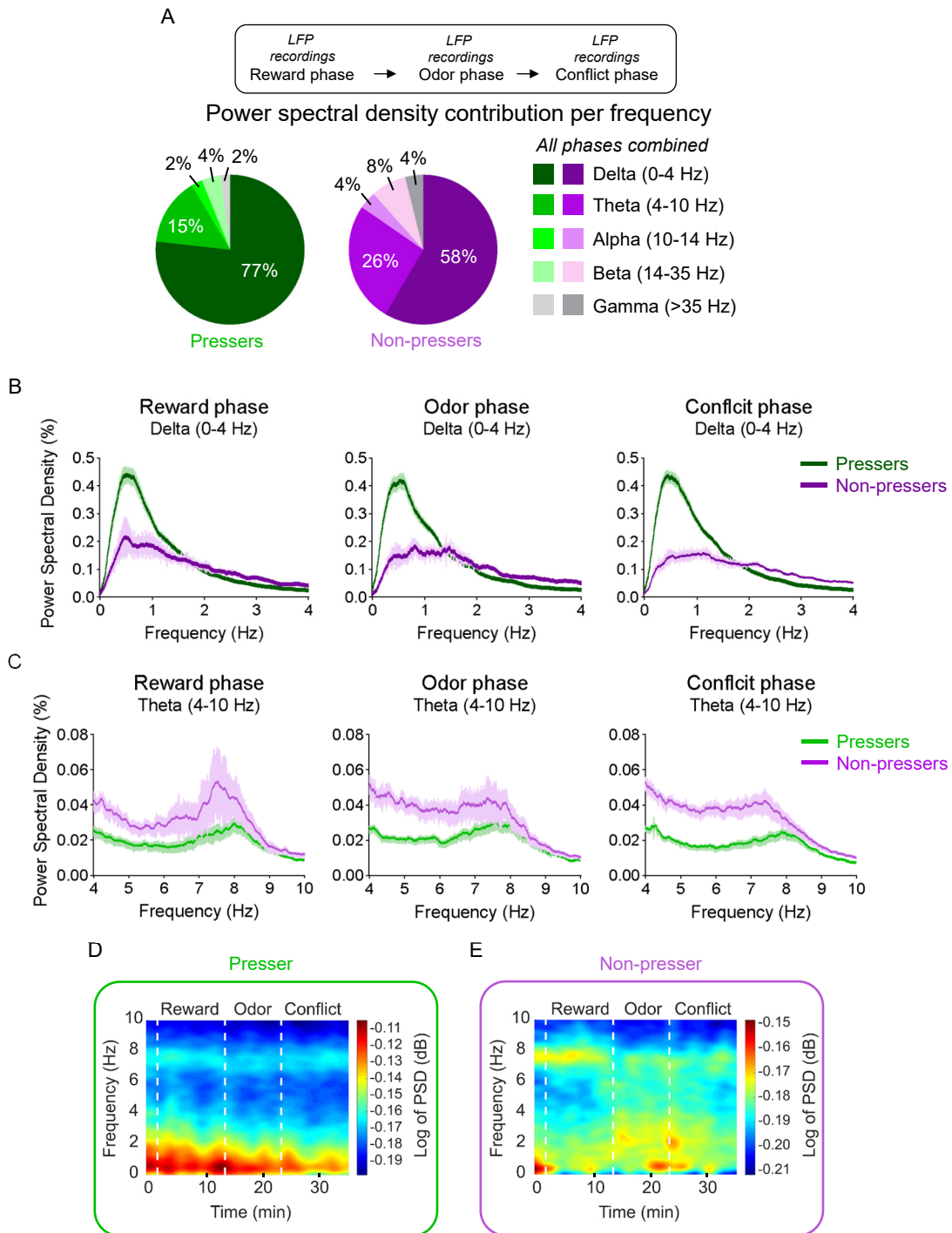


Figure 4. Pressers and Non-Pressers show significant differences in PL oscillations during the test session. (A) Power spectral density (PSD) contribution at different frequency bands. (B-C) Average of PSD (%) in the (B) delta (0-4 Hz) or (C) theta (4-10 Hz) bands in *Pressers* (green line, n = 25 rats) and *Non-Pressers* (purple line, n = 7 rats) during the (left) reward, (center) odor, and (right) conflict phases of the test session. *Pressers* showed increased power in the delta band, whereas *Non-Pressers* showed increased power in the theta band during the three phases of the test session (Unpaired Student's t-test comparing *Pressers* vs. *Non-Pressers*, all p's < 0.001). (D-E) Representative time-frequency spectrogram showing changes in the log of PSD (dB) for delta and theta bands in (D) *Pressers* and (E) *Non-Pressers* across the different phases of the session. All statistical analysis details are presented in table S1.

FIGURE 5

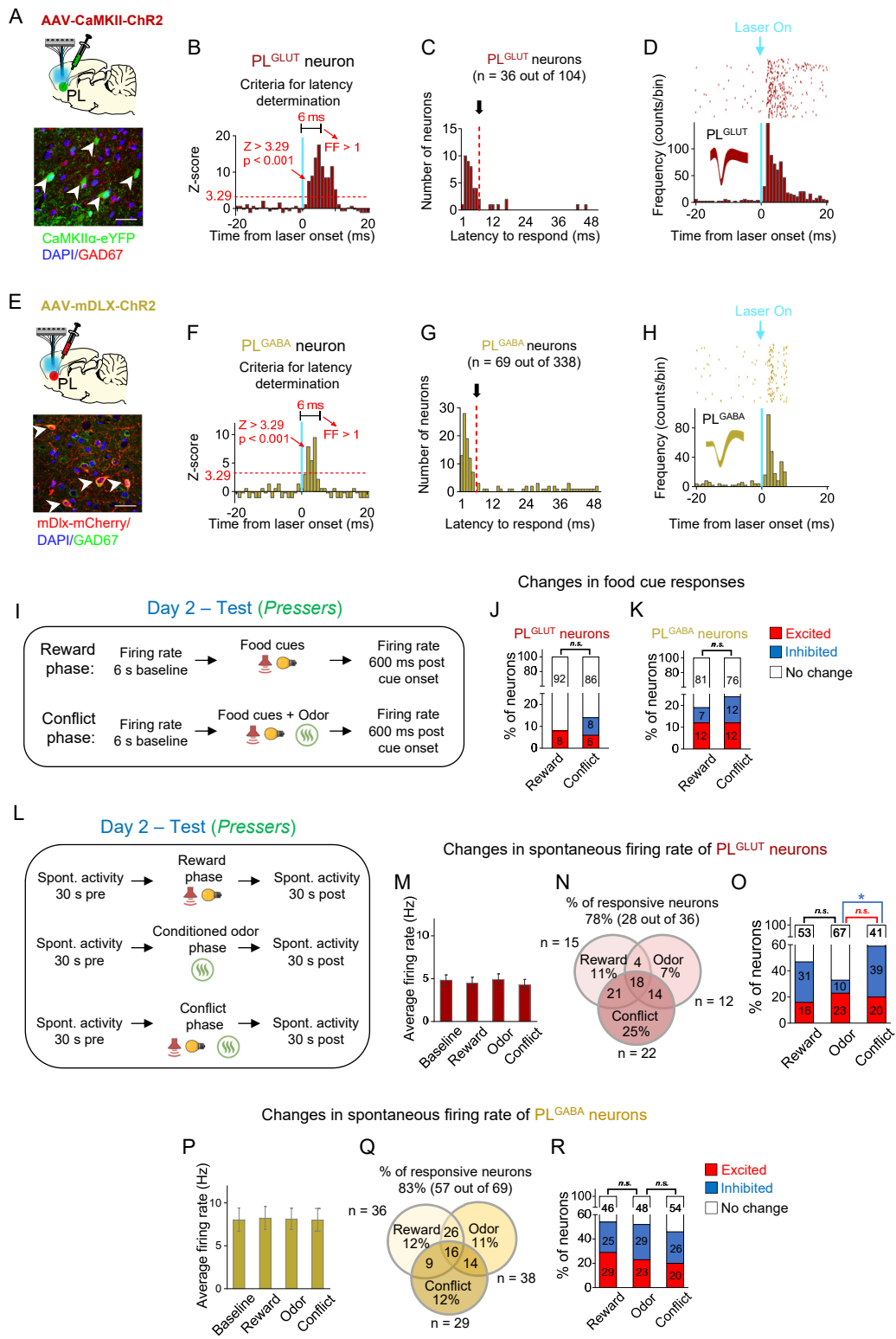


Figure 5. In pressers, PL^{GLUT} neurons show reduced spontaneous activity during the conflict phase. (A) Top, Schematic of viral infusion. Bottom, Representative immunohistochemical micrograph showing lack of colabeling (white arrows) between the ChR2 viral construct (green, AAV-CaMKII-ChR2-eYFP) and the GABA marker GAD67 (red), confirming that the use of a CaMKII promoter enables transgene expression favoring PL glutamatergic neurons. Scale bars: 25 μ m. (B-D) Photoidentification of PL^{GLUT} neurons. (B) Frequency histogram showing the latency of response to laser illumination for PL neurons (n = 36 photoidentified PL^{GLUT} neurons out of 104 recorded cells). Triangle method detection of cluster distribution revealed a separation of latency frequencies at 6 ms (see details in Methods section). (C) Cells with photoresponse latencies < 6 ms (identified as the first bin with Z-score > 3.29, p < 0.001, red dotted line) and high spike reliability during the 6 ms (FF, Fano Factor ratio > 1 compared to pre-laser baseline) were classified as PL^{GLUT} neurons (see details in Methods section). (D) Raster plot and peristimulus time histogram showing a representative PL^{GLUT} neuron responding to a 5 Hz train of laser stimulation. (E) Top, Schematic of viral infusion. Bottom, Representative immunohistochemical micrograph showing colabeling (white arrows) between the ChR2 viral construct (red, AAV-mDlx-ChR2-mCherry) and the GABA marker GAD67 (green), confirming that the use of a mDlx promoter enables transgene expression favoring PL GABA neurons. Scale bars: 25 μ m. (F-H) Photoidentification of PL^{GABA} neurons. (F) Frequency histogram showing the latency of response to laser illumination for PL neurons (n = 69 photoidentified PL^{GABA} neurons out of 338 recorded neurons). Triangle method detection of cluster distribution revealed a separation of latency frequencies at 6 ms (see details in Methods section). (G) Cells with photoresponse latencies < 6 ms (identified as the first bin with Z-score > 3.29, p < 0.001, red dotted line) and high spike reliability during the 6 ms (FF, Fano Factor ratio > 1 compared to pre-laser baseline) were classified as PL^{GABA} neurons (see details in Methods section). (H) Raster plot and peristimulus time histogram showing a representative PL^{GABA} neuron responding to a 5Hz train of laser stimulation. Vertical blue bars: laser onset. Bins of 1 ms. (I) Timeline of PL recordings for food cue responses in *Pressers* during test (12 food cues per phase). (J-K) Stacked bar showing the percentage of (J) PL^{GLUT} neurons or (K) PL^{GABA} neurons that changed their firing rates in response to food cues from the reward phase to the conflict phase. No significant differences were observed across the phases (Fisher Exact Test, all p's > 0.05; n.s. = non-significant). (L) Timeline of PL recordings for spontaneous activity in *Pressers* during test. (M) Average firing rate of PL^{GLUT} neurons across the different phases of test. (N) Venn diagram showing the percentage of responsive PL^{GLUT} neurons (28 out of 36 neurons) by events. (O) Stacked bar showing the percentage of PL^{GLUT} neurons that changed their spontaneous firing rates across the different phases of the test. PL^{GLUT} neurons did not change their firing rates from the reward to the odor phase (Fisher Exact Test, inhibited in Reward phase: 10 neurons, inhibited in Odor phase: 3 neurons, p = 0.063), but were subsequently inhibited from the odor to the conflict phase (Fisher Exact Test, inhibited in Odor phase: 3 neurons, inhibited in Conflict phase: 14 neurons, p = 0.0046). (P) Average firing rate of PL^{GABA} neurons across the different phases of test. (Q) Venn diagram showing the percentage of responsive PL^{GABA} neurons (57 out of 69 neurons) by events. (R) Stacked bar showing the percentage of PL^{GABA} neurons that changed their spontaneous firing rates across the different phases of the test. No significant differences were observed across the phases (Fisher Exact Test, all p's > 0.05; n.s. = non-significant). All statistical analysis details are presented in table S1. See also Supplementary Figs. 7, 8, and 9.

FIGURE 6

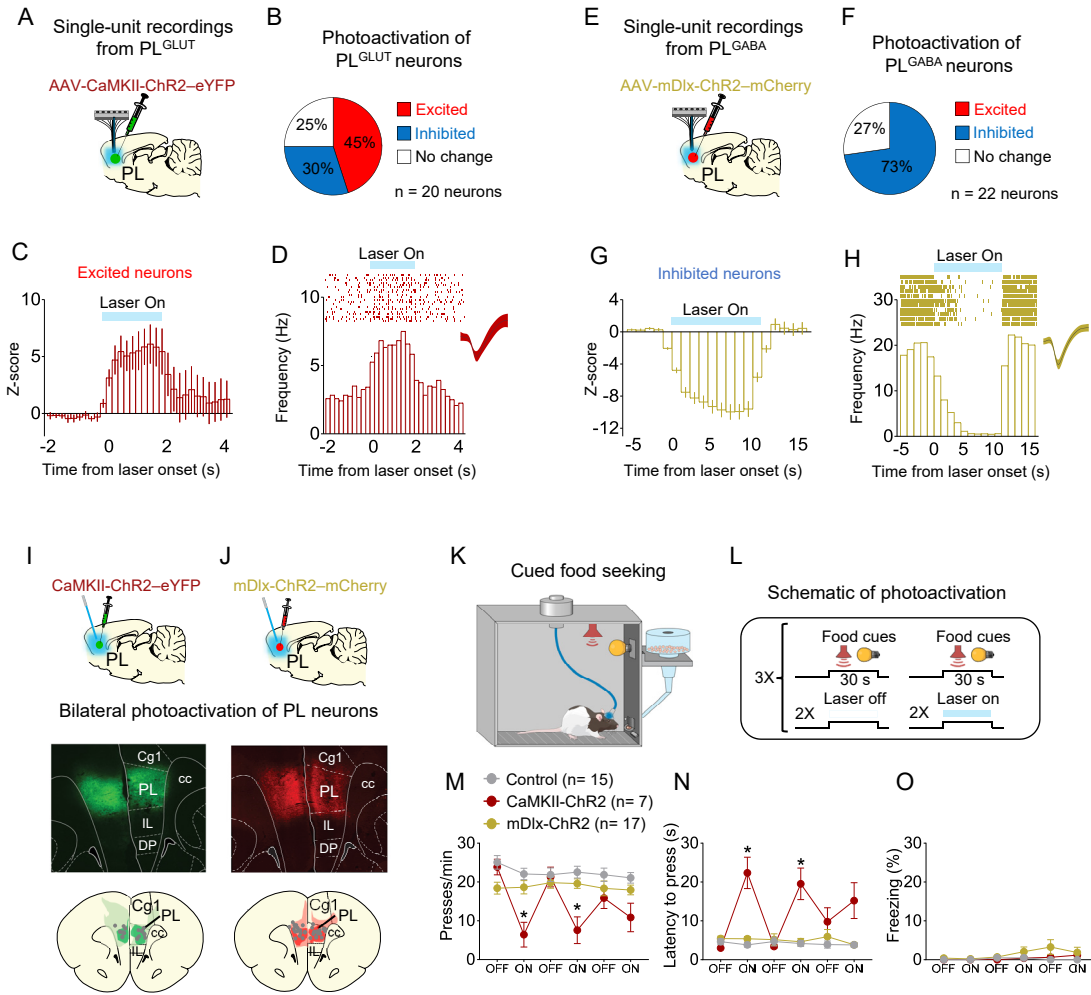


Figure 6. Photoactivation of PL^{GLUT}, but not PL^{GABA}, neurons suppresses reward seeking in a neutral context. (A) Schematic of viral infusion and recordings in PL. **(B)** Changes in PL firing rate with illumination of PL^{GLUT} neurons in rats expressing AAV-CaMKII-ChR2-eYFP in PL (n= 20 neurons). **(C)** Average PSTH of PL neurons that were excited during laser illumination of PL^{GLUT} neurons. **(D)** Raster plot and peri-stimulus time histogram (PSTH) of representative PL neuron showing excitatory responses to illumination in rats expressing AAV-CaMKII-ChR2-eYFP in PL. **(E)** Schematic of viral infusion and recordings in PL. **(F)** Changes in PL firing rate with illumination of PL^{GABA} neurons in rats expressing AAV-mDlx-ChR2-mCherry in PL (n= 22 neurons). **(G)** Average PSTH of PL neurons that were inhibited during laser illumination of PL^{GABA} neurons. **(H)** Raster plot and PSTH of representative PL neuron showing inhibitory responses to illumination in rats expressing AAV-mDlx-ChR2-mCherry in PL. **(I-J)** Representative micrograph showing the expression of (I) CaMKII-ChR2-eYFP or (J) mDlx-ChR2-mCherry in PL and schematic of optical fiber location (gray dots) in the same region (compressed across different antero-posterior levels of PL). Green or red areas represent the minimum (dark) and the maximum (light) viral expression into the PL. **(K-L)** Schematic and timeline of PL photoactivation during the cued food seeking test in a neutral context. **(M-N)** Optogenetic activation of PL^{GLUT} neurons (CaMKII-ChR2, dark red circles, n = 7), but not PL^{GABA} neurons (mDlx-ChR2, gold circles, n = 17), reduced the (M) frequency of lever presses ($F_{(10, 180)} = 7.009$, $p < 0.001$, Bonferroni *post-hoc*, CaMKII-ChR2 vs. Control, all laser on periods - $p < 0.01$; mDlx-ChR2 vs. Control, all laser on periods - $p > 0.05$) and increased (N) the latency for the first press ($F_{(10, 180)} = 9.931$, $p < 0.001$, CaMKII-ChR2 vs. Control, all laser on periods - Bonferroni *post-hoc*, $p < 0.001$; mDlx-ChR2 vs. Control, all laser on periods, $p > 0.05$). **(O)** Optogenetic activation of PL neurons did not alter freezing behavior ($F_{(10, 180)} = 1.124$, $p = 0.346$). Blue shaded area represents laser-on trials (PL^{GLUT}: 5 Hz, PL^{GABA}: 20 Hz; 5ms pulse width, 7-10 mW, 30 s duration). Data shown as mean \pm SEM. Each circle represents the average of two consecutive trials. Two-way repeated-measures ANOVA followed by Bonferroni *post-hoc* test. All * p 's < 0.05 . All statistical analysis details are presented in table S1.

FIGURE 7

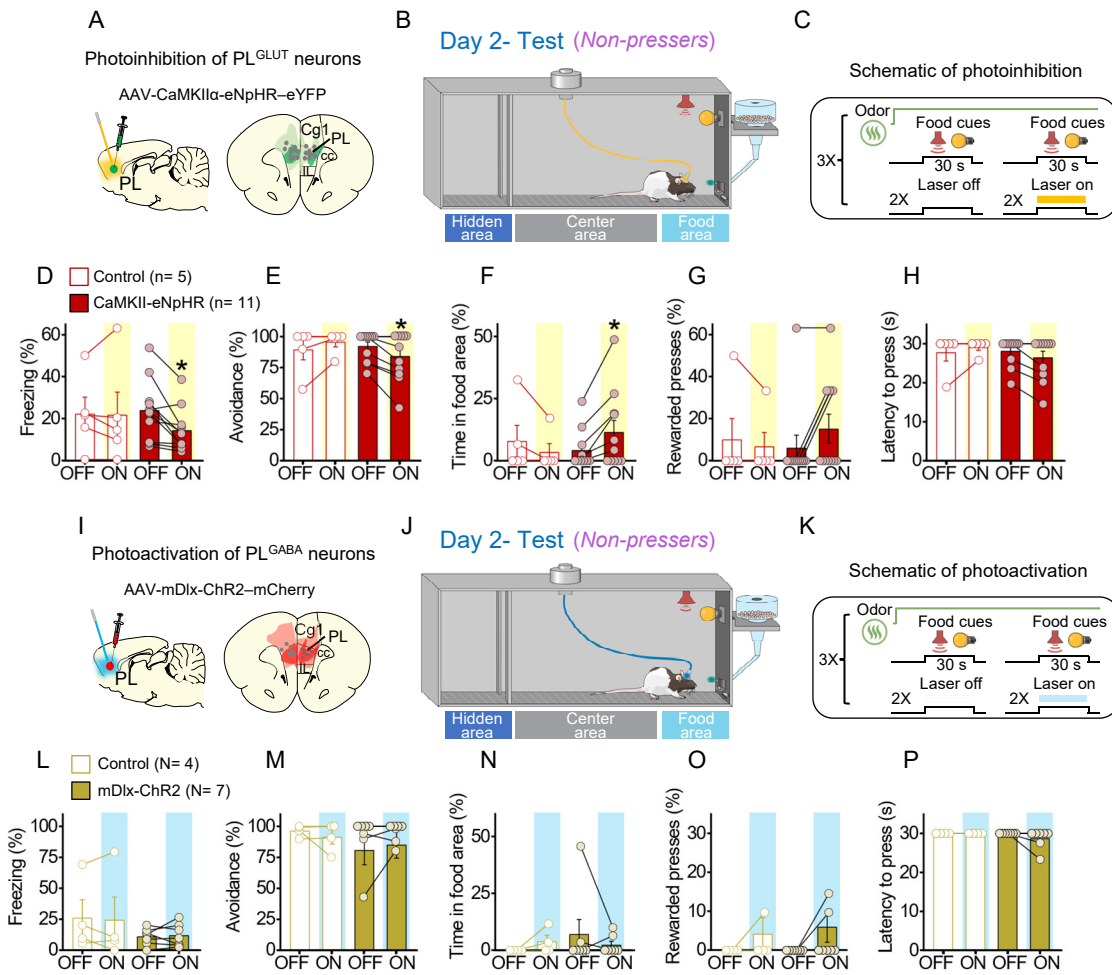


Figure 7. Photoinhibition of PL^{GLUT} neurons during conflict reduces freezing and increases food approaching in *Non-Pressers*. **(A)** Schematic of AAV-CaMKII-eNpHR-eYFP virus infusion in PL and location of optical fibers (gray dots) in the same region (compressed across different antero-posterior levels of PL). Green areas represent the minimum (dark) and the maximum (light) viral expression into the PL. **(B-C)** Schematic and timeline of the approach-avoidance conflict test during optogenetic inhibition of PL^{GLUT} neurons. **(D-H)** Photoinhibition of PL^{GLUT} neurons (CaMKII-eNpHR, red bars, n = 11) during the conflict test reduced the percentage of time rats spent (D) freezing (Wilcoxon test, W = -64, laser off vs. laser on, p = 0.0020, Mann-Whitney Test, U = 18 Control vs. CaMKII-eNpHR, p = 0.319) and (E) avoiding the odor area (Wilcoxon test, W = -21, laser off vs. laser on, p = 0.031; Mann-Whitney Test, U = 19.5 Control vs. CaMKII-eNpHR, p = 0.365), and increased the percentage of time rats spent in the (F) food area (Wilcoxon test, W = 21, laser off vs. laser on, p = 0.031; Mann-Whitney Test, U = 17 Control vs. CaMKII-eNpHR, p = 0.221) during the conflict test without altering (G) the number of lever presses (Wilcoxon test, W = 6, laser off vs. laser on, p = 0.250; Mann-Whitney Test, U=22.5 Control vs. CaMKII-eNpHR, p=0.697) and (H) the latency to press (Wilcoxon test, W = -10, laser off vs. laser on, p = 0.125; Mann-Whitney Test, U = 21 Control vs. CaMKII-eNpHR, p = 0.357). Laser stimulation did not alter behaviors in controls (eYFP-control virus, white bars, n= 5, Wilcoxon test, Freezing: W = 3, p = 0.812, avoidance: W = 3, p = 0.500, food area: W = -3, p = 0.500, lever presses: W = -1, p = 0.999, latency to press: W = 1, p = 0.999). For all Shapiro-Wilk normality test, p < 0.05. **(I)** Schematic of AAV-mDlx-ChR2-mCherry virus infusion in PL and location of optical fibers (gray dots) in the same region (compressed across different antero-posterior levels of PL). Red areas represent the minimum (dark) and the maximum (light) viral expression into the PL **(J-K)** Schematic and timeline of the approach-avoidance conflict test during optogenetic activation of PL^{GABA} neurons. **(L-P)** Photoactivation of PL^{GABA} neurons during the conflict test did not alter rats' behavior in the mDlx-ChR2 group (gold bars, n= 7) or in the control group (eYFP-control virus, white bars, n = 4, Wilcoxon and Mann-Whitney tests, all p's > 0.05). For all Shapiro-Wilk normality test, p < 0.05. PL neurons were illuminated from cue onset until the animals pressed the lever or from cue onset until the end of the 30 s cues if the animals didn't press the lever (PL^{GLUT}: 5 Hz, PL^{GABA}: 20 Hz; 5 ms pulse width, 7-10 mW). Data shown as mean ± SEM. Each bar represents the average of six trials alternated in blocks of 2. All * p's < 0.05. All statistical analysis details are presented in table S1. See also Supplementary Fig 10.

FIGURE 8

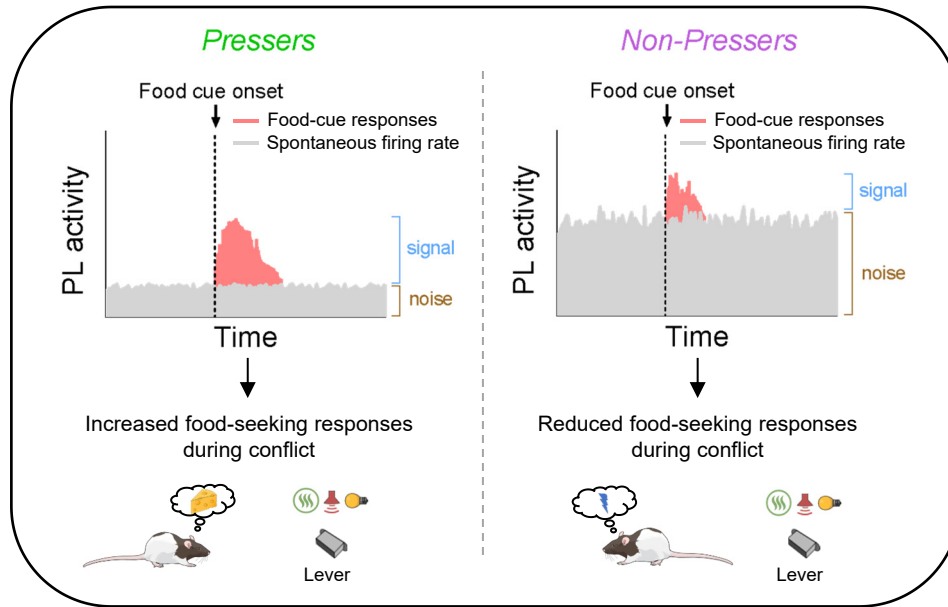


Figure 8. Schematic showing differences in food-cue responses and spontaneous firing rate of PL neurons in *Pressers* and *Non-Pressers*. Left, *Pressers* showed reduced spontaneous firing rate and increased food-cue responses in PL neurons during the conflict test, which may have resulted in higher signal-to-noise ratio and increased food-seeking responses. Right, *Non-Pressers* showed increased spontaneous firing rate and reduced food-cue responses in PL neurons during the conflict test, which may have resulted in lower signal-to-noise ratio and reduced food-seeking responses.